Journal of Hazardous Materials 474 (2024) 134819

Contents lists available at ScienceDirect

Journal of Hazardous Materials

journal homepage: www.elsevier.com/locate/jhazmat

Superior sequence-controlled poly(L-lactide)-based bioplastic with tunable seawater biodegradation

Manjie He, Yu-I. Hsu *, Hiroshi Uyama *

Department of Applied Chemistry, Graduate School of Engineering, Osaka University, 2-1 Yamadaoka, Suita, Osaka 565-0871, Japan

HIGHLIGHTS

- PLA-based bioplastic with tunable marine biodegradability.
- Exploring PEG-PLA with alternating or random structures impacts its performance.
- Alternating PEG-PLA showed superior mechanical properties in dry and wet states.
- The introduction of PEG promoted PLA biodegradation in proteinase K and seawater.
- PEG-PLA exhibited the fastest degradability in reported marine-degradable polymers.

GRAPHICAL ABSTRACT

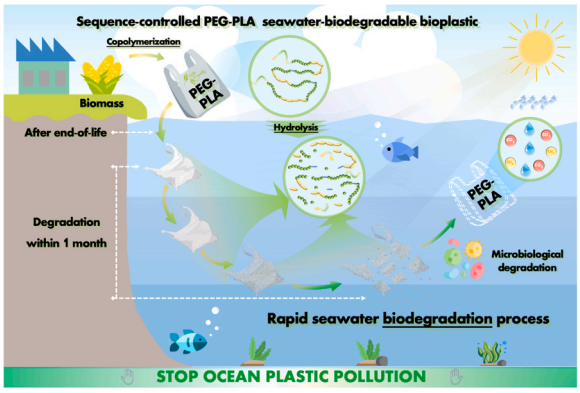

ARTICLE INFO

Keywords:
BOD analysis
Degradation mechanism
Tunable seawater biodegradability
PLA-based bioplastics

ABSTRACT

Developing superior-performance marine-biodegradable plastics remains a critical challenge in mitigating marine plastic pollution. Commercially available biodegradable polymers, such as poly(L-lactide) (PLA), undergo slow degradation in complex marine environments. This study introduces an innovative bioplastic design that employs a facile ring-opening and coupling reaction to incorporate hydrophilic polyethylene glycol (PEG) into PLA, yielding PEG-PLA copolymers with either sequence-controlled alternating or random structures. These materials exhibit exceptional toughness in both wet and dry states, with an elongation at break of 1446.8% in the wet state. Specifically, $PEG_{4k}PLA_{2k}$ copolymer biodegraded rapidly in proteinase K enzymatic solutions and had a significant weight loss of 71.5% after 28 d in seawater. The degradation primarily affects the PLA segments within the PEG-PLA copolymer, as evidenced by structural changes confirmed through comprehensive characterization techniques. The seawater biodegradability, in line with the Organization for Economic Cooperation and Development 306 Marine biodegradation test guideline, reached 72.63%, verified by quantitative biochemical oxygen demand analysis, demonstrating rapid chain scission in marine environments. The capacity of PEG-PLA bioplastic to withstand DI water and rapidly biodegrade in seawater makes it a promising candidate for preventing marine plastic pollution.

* Corresponding authors.
E-mail addresses: yuihsu@chem.eng.osaka-u.ac.jp (Y.-I. Hsu), uyama@chem.eng.osaka-u.ac.jp (H. Uyama).

https://doi.org/10.1016/j.jhazmat.2024.134819
Received 2 April 2024; Received in revised form 26 May 2024; Accepted 3 June 2024
Available online 4 June 2024

1. Introduction

Plastic production has surged since 1950 to reach 460 million metric tons (MT), with packaging waste accounting for 1.41 MT in 2019. About 50% of plastics are discarded after a single use, resulting in an annual average of 4.8 to 12.7 MT of plastic waste entering marine ecosystems [1,2]. This has significant implications for human health, as microplastics may accumulate in the human body through the food chain [3–5]. Unless practical innovations in global plastic production and waste management are implemented, approximately 53 MT of marine plastic waste will be generated by 2030 [6,7]. Thus, it is imperative to develop sustainable and marine-biodegradable alternatives [8].

Conventional biodegradable polymers, such as bio-based poly(lactic acid) (PLA) [9,10], have garnered significant attention as biodegradable material over the past half-century due to their desirable properties, including heat resistance, excellent mechanical strength, and high transparency compared to several common plastics. However, their biodegradation requires specific compost conditions, which means they cannot biodegrade in all natural environments [2]. The degradation rate of these polymers decreases significantly in seawater due to limited marine microbial community and low temperatures [11]. The weight loss of PLA is only approximately 1% after 400 d in seawater [12], attributed to its high glass transition temperature (T_g) [9,13].

Given the presence of complicated and uncontrollable external factors, researchers have focused on the intrinsic degradation factors of polymers in marine environments [14–16]. A practical approach involves blending or copolymerizing hydrophilic materials with biodegradable plastics to achieve higher seawater degradability and avoid the formation of microplastics. Huang et al. [17] enhanced the degradation of PLA in seawater by introducing water-soluble polyvinyl alcohol as a filler. Chen et al. utilized the readily degradable property of poly (lactic-co-glycolic acid) (PLGA) to improve the degradation efficiency of PLA in seawater by blending PLGA with PLA [18]. In these composites, the hydrophilic domains degrade predominantly due to the incorporated material, while the matrix polymer remains stable. In addition, marine degradable polymers can be chemically modified to enhance their hydrolytic or enzymatic degradation rates, affecting their crystallinity and mechanical properties [13,19–21]. Rheinberger et al. introduced hydroxyethoxy side group phosphate esters to serve as "breaking points" in PLA through an RNA-like endoester exchange reaction to improve the degradation of PLA [22]. The integration of hydrophilic aliphatic units proved efficient in enhancing degradability. Polyhydroxyalkanoates (PHAs) are the most well-known marine biodegradable biopolymers, as they can be degraded by many bacteria and fungi, resulting in a relatively fast degradation rate. They are suitable for reducing the long-term impact of marine plastic waste [23]. However, PHAs are typically produced through bacterial fermentation, which leads to high production costs. Low heat distortion temperature and poor gas barrier properties limit their development [24]. Thus, improving the hydrophilicity and enzyme affinity of materials plays a crucial role in their seawater-biodegradability.

Polyethylene glycol (PEG) is widely used for its hydrophilic, flexible,

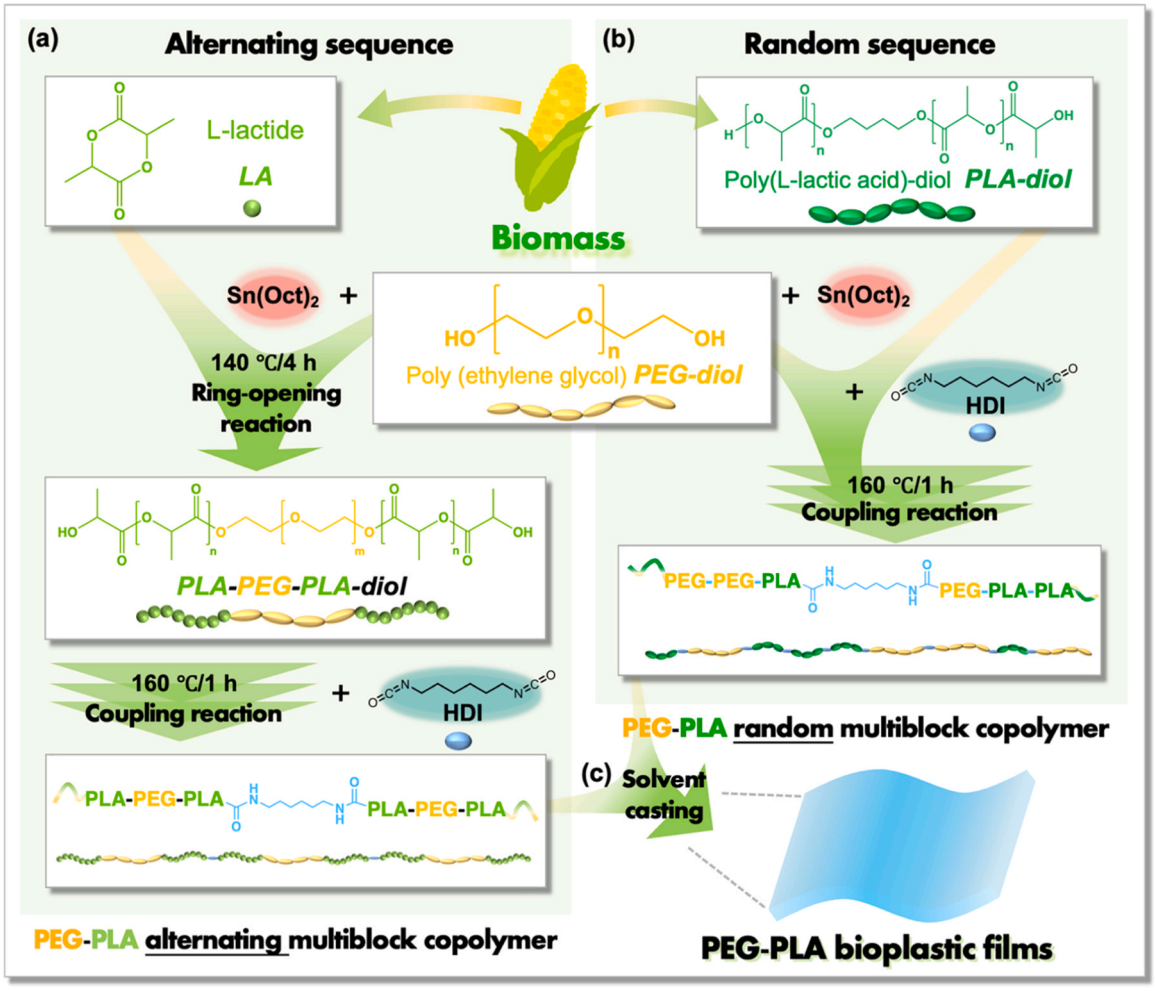

Scheme 1. Schematic representation of the synthesis of PEG-PLA (a) alternating and (b) random multiblock copolymers and (c) films created through solvent casting.

and biocompatible properties, and it has been approved by the FDA for use in biomedical applications [25]. Wolf et al. demonstrated that the degradation of poly(alkylphosphate) modified with PEG was accelerated under artificial seawater conditions [26]. Therefore, incorporating PEG may generate more potential "breaking points" in the backbone and increase the hydrophilicity of the copolymer, thus leading to a rapid seawater degradation rate. Also, it can help improve the inherent brittleness and low toughness of PLA [27]. Additionally, PEG-PLA amphiphilic block copolymer nanoparticles and multiblock systems have been extensively studied, such as drug carriers in biomedical fields, and have demonstrated their enzymatic biodegradability [28–30]. Our group recently reported that PEG-PLA copolymers present superior water absorption and durability in DI water, which are considerably influenced by the PEG content [31]. To the best of our knowledge, there are some studies about new seawater-degradable polymers, but few employ natural seawater for the microorganisms. Importantly, no research utilizes the features of PEG-PLA copolymers for marine biodegradability.

In this research, due to improving the degradation of a material often compromises its mechanical properties, the primary goal was to enhance and tunable the biodegradability of PLA in seawater and maintain their superior toughness even in DI water. PEG-PLA copolymer bioplastics with sequence-controlled alternating or random structures and PLA homopolymer were synthesized with high yields and purity through a robust ring-opening (ROP) and coupling process comprising PLA and PEG as building blocks. The effect of the PEG content in the alternating and random molecular chain structures on the hydrophilic, thermal, and mechanical properties of PLA-based bioplastics was investigated. The dynamic degradation behavior of PEG-PLA in Tris-HCl buffer solution, proteinase K solution, and seawater was also carefully explored. A biodegradability of 72.63% was obtained through a quantitative biochemical oxygen demand (BOD) analysis [32]. This confirmed that the PEG incorporated in the PLA backbone accelerated the chain scission of the material in seawater within 28 d for the adjusted and readily biodegradation. The PEG-PLA alternating copolymers showed a balance between performance retention and marine biodegradability in practical applications. The biodegradation prioritized the PLA segments within the PEG-PLA copolymer, as evidenced by structural changes verified through comprehensive characterization techniques. The rapid seawater biodegradation rate and superior mechanical properties of PEG-PLA make it a prime candidate for seawater-biodegradable polymers, providing a new perspective for its use in the packaging, medical, and agricultural industries.

2. Materials and methods

2.1. Materials

Poly(ethylene glycol) (PEG, M_n = 4000 Da, GR grade), aniline (GR grade), proteinase K, diethyl ether (DE, GR grade), chloroform ($CHCl_3$, GR grade), toluene (super dehydrate, organic synthesis grade), and tin (II) 2-ethylhexanoate ($Sn(Oct)_2$, > 95%) were supplied by Wako Pure Chemical Industries (Osaka, Japan). PLA-diol (M_n = 2000 Da, 3000 Da) was purchased from HighChem Co., Ltd. (Tokyo, Japan). 1,6-Hexamethylene diisocyanate (HDI, >98%) was obtained from the Tokyo Chemical Industry Co., Ltd. (Tokyo, Japan). A pH 8.5 buffer solution of 1 mol L^{-1} Tris hydrochloride (Tris-HCl) was provided by Sigma-Aldrich (Massachusetts, U.S.A.). All reagents were used as received unless otherwise stated. $Sn(Oct)_2$ was diluted in dry toluene and stored in a glass volumetric flask under a nitrogen atmosphere before use. Deionized (DI) water purified using a Milli-Q system (Millipore Inc., Milford, MA, USA) was used for all experiments.

2.2. Synthesis of PEG-PLA multiblock copolymers with alternating and random structures

A series of PEG-PLA alternating multiblock copolymers with various compositions were prepared via a facile bulk polymerization technique (*i.e.*, ROP and coupling process), as shown in Scheme 1a. Further information is provided in our previous study [31]. The synthesis procedure for the PEG-PLA random multiblock copolymers is shown in Scheme 1b. A 200 mL three-necked round-bottom flask was filled with PLA-diol and PEG-diol at a molar ratio of 2:1 under a nitrogen atmosphere. The mixture was stirred for 3 h at ambient temperature under a vacuum of less than 30 Pa to remove water and oxygen. Subsequently, a toluene solution containing $Sn(Oct)_2$ equivalent to the 1 mol% of the PEG-diol component was injected. The resultant system was then stirred under vacuum at ambient temperature for 1 h to ensure complete mixing, followed by heating to 160 °C. A fixed 1:1.2 molar ratio of total PLA-diol to PEG-diol was used, and HDI was added to the reaction system dropwise. Vigorous mechanical stirring was performed for 1 h to confirm that the coupling reaction was completed. Meanwhile, the procedure for the random sequence was also used to synthesize PLA homopolymers (Fig. S1). To purify the PEG-PLA alternating and random multiblock copolymers and PLA homopolymers, the crude products were first dissolved in $CHCl_3$, precipitated by DE, and dried under vacuum for 24 h at ambient temperature to remove residual solvents, and kept well for characterization. The nomenclature for all the synthesized copolymers and homopolymers is given as PEGxPLAy-*a/r/h*, where 'x' and 'y' represent the molecular weights of PEG and PLA chain segments, respectively; the suffixes 'a', '*r*', and '*h*' denote alternating copolymers, random copolymers, and homopolymers, respectively.

2.3. Preparation of PEG-PLA multiblock copolymer films

PEG-PLA multiblock copolymer films with thicknesses of 0.3–0.4 mm were fabricated by solvent casting from the purified products in a horizontal Teflon mold using $CHCl_3$. In a fume hood, the solvent was evaporated naturally at ambient temperature for 2–3 d. The obtained films (Scheme 1c) were moved to an oven at 25 °C for 24 h and carefully sealed for testing.

2.4. Water uptake ratio (WUR) of PEG-PLA multiblock copolymer films

The water uptake ratio (WUR) was evaluated using Milli-Q water. Dry film samples (2 × 2 cm) were prepared in quintuplicate, and their initial dry weights (W_d) were recorded. The samples were fully immersed in water at 25 °C. After a predetermined period, the samples were carefully extracted using tweezers. The extra surface water was gently blotted off with tissue paper, and the wet weights of the samples (W_s) were promptly measured. The WUR was calculated based on the initial dry weight of the film samples using Eq. (1).

$$\boldsymbol{WUR}\ (\%) = \frac{\boldsymbol{W_s} - \boldsymbol{W_d}}{\boldsymbol{W_d}} \times \mathbf{100\%} \quad (1)$$

Based on Eq. (1), the WUR was calculated for the five samples and averaged. This approach ensured quantification of the water durability of materials, facilitating a comparison of the hydrophilic properties of different films.

2.5. Degradation of PEG-PLA multiblock copolymer films in different conditions

2.5.1. Hydrolytic degradation and enzymatic biodegradation

The degradation of PLA is facilitated by proteinase K [33,34]. Thus, the enzymatic degradation behavior of PEG-PLA films was characterized by proteinase K. The initial weights of the films were recorded (W_0), and the films were then immersed in 25 mL of 0.05 mol L^{-1} Tris-HCl buffer solution (pH 8.5) containing proteinase K. The procedure was carried out over 120 h at 37 °C to evaluate the degradation behavior comprehensively. After incubation, the films were carefully removed from the solution and gently rinsed with DI water to remove any residual enzyme solution. The films were then lyophilized and weighed (W_t). The

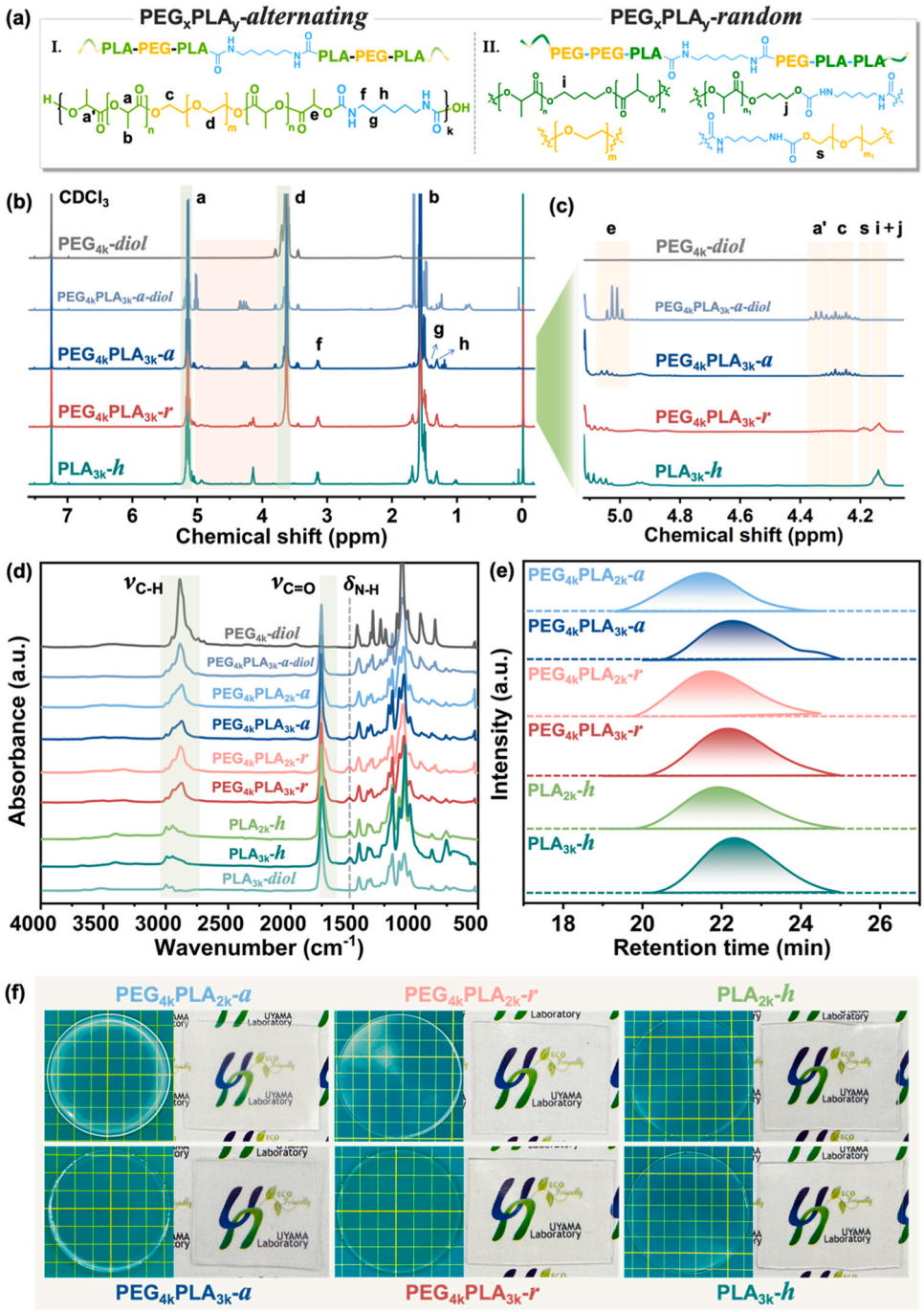

Fig. 1. (a) Chemical structural units of PEG-PLA multiblock copolymers with alternating (i) and random (ii) structures. Original (b) and enlarged (c) ^{1}H NMR spectra of PEG-PLA copolymers and PLA homopolymers. (d) FT-IR spectra of PEG-PLA copolymers and PLA homopolymers. (e) GPC profiles of PEG-PLA copolymers and PLA homopolymers. (f) Corresponding macro appearance.

enzymatic biodegradability of the multiblock copolymers was quantitatively assessed using Eq. (2).

$$\textit{Residue weight}\ (\%) = \frac{W_t}{W_0} \times 100\% \quad (2)$$

Degradation tests were conducted in quintuplicate to ensure statistical relevance, and the results are presented as mean values.

2.5.2. *Marine biodegradation in seawater based on BOD analysis*

A natural seawater sample was collected near Koshien Hama in Osaka Bay (N34°42′20.36′, E135°21′12.44′) on October 29, 2023; the seawater temperature was 21.7 °C. The water was then transferred to a cleaned 5 L plastic jerry can wrapped in aluminum foil to keep out light and delivered to the Uyama laboratory at the Suita campus of Osaka University within 4 h (Fig. S2).

Closed-bottle tests were performed in a temperature-controlled BOD reactor (Velp Scientifica™ RESPIROMETRIC Sensor System 6, Italy) according to the Organization for Economic Cooperation and Development Marine biodegradation test guideline (OECD 306) [35]. This technique quantifies the aerobic biodegradation capability of organic substances by tracking the oxygen uptake of microorganisms at 20 °C in the dark, which was achieved by covering the reactors with aluminum foil for 28 d under constant stirring (Fig. S2). Automatic pressure results from conversion in BOD data. The RESPIROMETRIC Sensor transmits

data directly to the PC, enabling real-time monitoring of the analysis curve.

Each film sample and an aniline reference (approximately 10 mg each) were weighed (W_0) and placed separately in a 300 mL BOD reactor, and test water (100 mL) was poured into the reactor as an inoculum. Subsequently, mineral supplements of 25 mg NH_4Cl, 5 mg $NaHPO_4$, 0.5 mg N-allylthiourea, and 0.1 mL of a buffer solution were added to the test water. The buffer solution comprised 33.30 g of $NaHPO_4{\cdot}2\,H_2O$, 21.75 g of K_2HPO_4, 8.50 g of KH_2PO_4, and 0.50 g of NH_4Cl per liter. Then, BOD data were recorded and processed using a computer system at regular intervals (day). The BOD biodegradability of the films was calculated using Eq. (3) [36].

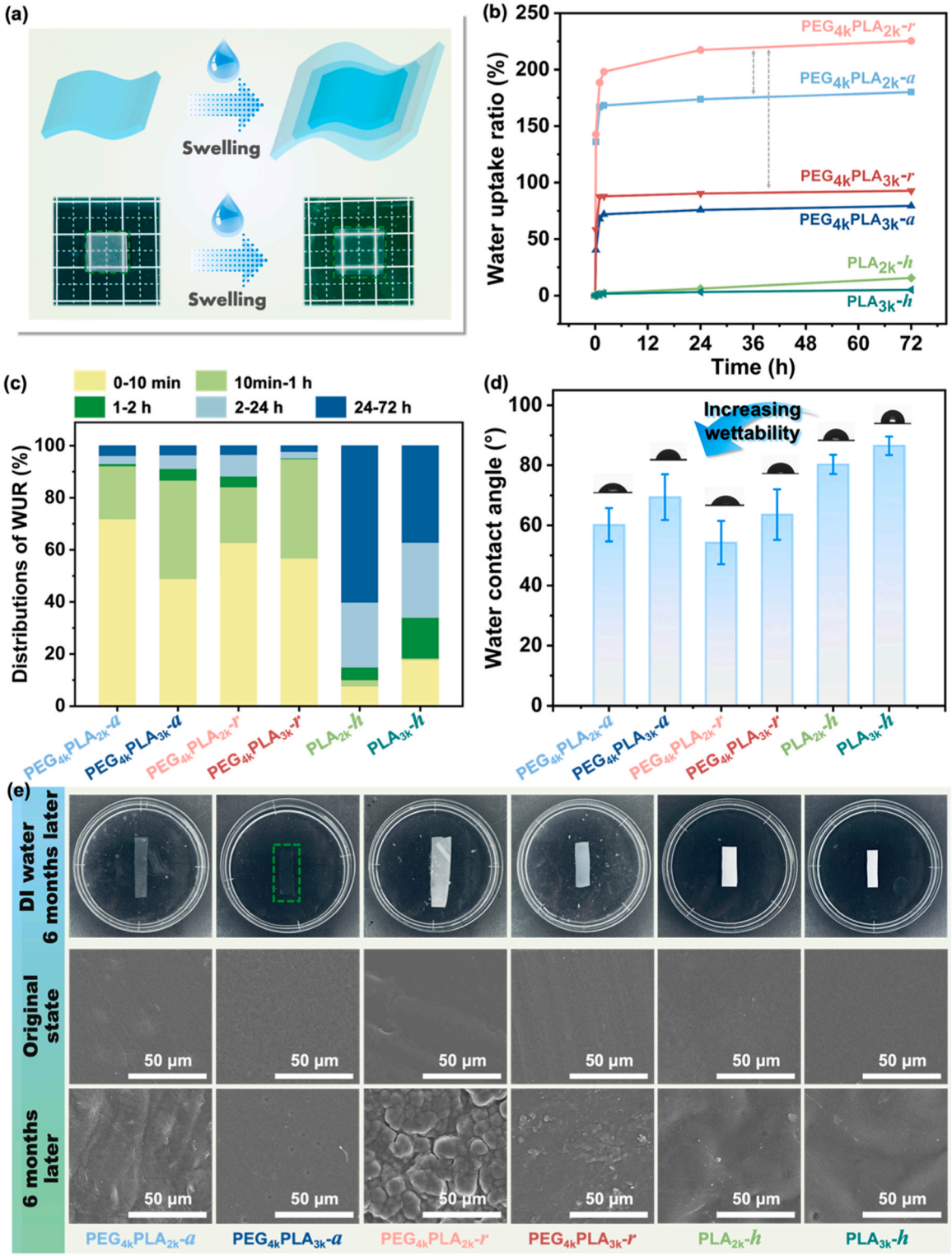

Fig. 2. (a) Schematic illustration of the water uptake process of PEG-PLA and PLA films. (b) WUR profile of PEG-PLA and PLA films within 72 h. (c) WUR distributions of all samples after different immersion periods. (d) Water contact angles of PEG-PLA and PLA films. (e) Appearance and microstructures of PEG-PLA and PLA films after 6 months DI water soaking.

$$\textbf{BOD Biodegradability}\ (\%) = \frac{BOD_t - BOD_b}{ThOD} \times 100\% \quad (3)$$

where BOD_t is the BOD of the test solution, BOD_b is the BOD of the control blank, and *ThOD* represents the theoretical oxygen demand. An organic microelemental analyzer (MT-6, Yanaco Co., Ltd., Kyoto, Japan) was used to determine the C, H, N, and O contents of the samples. The obtained results were then used to calculate the *ThOD*. Two samples were evaluated in each BOD test. The BOD biodegradability of each sample was calculated as the average of the three results.

After incubation for 28 d, the films were carefully removed from the solution and gently washed with DI water to remove any residual seawater. The films were then lyophilized and weighed again (W_t). The dried films were used for characterization and testing. After seawater degradation, the residual weights of the samples were calculated using Eq. (2). Moreover, the M_n, chemical structure, composition, and thermal properties were evaluated using corresponding methodologies.

The characterization and measurements are described in more detail in the Supporting Information **(Experimental Techniques Section)**.

3. Results and discussion

PEG has been reported to produce PLA-PEG-PLA triblock copolymers via ROP, progressing rapidly. However, studies on the reaction between PLA-PEG-PLA short-chain segments (PLA units < 50) and isocyanate to generate polyurethane are limited. Scheme 1 illustrates our development of PEG-PLA multiblock copolymers with short PLA chain segments. This approach aimed to reduce marine pollution by enhancing abrasion resistance and durability under daily use and wet environments while facilitating rapid degradation in marine environments. By manipulating the copolymer structure and composition, we intended to balance mechanical properties and DI durability with rapid and controlled seawater biodegradability.

This study is expected to design a PLA-based bioplastic capable of rapid marine biodegradation while maintaining exceptional DI durability for various daily applications. Achieving a balance between toughness, flexibility, and hydrophilicity is crucial. This was accomplished by incorporating hydrophilic and flexible PEG into PLA by tailoring the EG/LA feed ratio. The flexible PEG enhanced copolymer hydrophilicity and toughness. Additionally, specific crystallization ability was required to enhance mechanical properties. Thus, we focused on PEG-diol with 4000 g mol^{-1} to meet these design requirements.

3.1. Chemical structures of PEG-PLA multiblock copolymers

The different constitutive repeating units of the PEG-PLA copolymers are depicted in Fig. 1a, illustrating alternating (i) and random (ii) blocks. ^{1}H NMR spectroscopy was used to verify the chemical structures and segment compositions. Table S1 lists the corresponding L-lactide conversion, M_n, and weight fractions (F). Typical ^{1}H NMR spectra of PEG-PLA and PLA are shown in Fig. 1b, where several signals can be distinguished. The strong proton peaks appearing at ***a*** **(CH, δ_m = 5.10–5.20 ppm)** and ***b*** **(CH$_3$, δ_d = 1.45–1.60 ppm)** are attributed to the methine and methyl protons of PLA, respectively. The chemical shift of ***d*** **(CH$_2$, δ_t = 3.60–3.70 ppm)** is assigned to the methylene protons on the backbone of PEG. Peak ***f*** **(CH$_2$-CH$_2$-<u>CH$_2$</u>-NH-CO, δ_q = 3.10–3.20 ppm)** is related to the methylene in the isocyanate after the coupling reaction, which implies the formation of a urethane linkage in the PEG-PLA and PLA. In addition, it is apparent in Fig. 1c that distinct chemical shifts of corresponding samples are observable in the magnified ^{1}H NMR spectra. Specifically, peaks **i**+***j*** **(-O-<u>CH$_2$</u>-CH$_2$-CH$_2$-CH$_2$-O-, δ_t = 4.13–4.17 ppm)** are exclusively present in the random-structure PEG-PLA copolymers and PLA homopolymer. This specificity is attributed to the PLA segments, which undergo direct ring-opening polymerization initiated by 1,4-butanediol and are subsequently terminated with butanediol [37]. The presence of the ***c***, ***a'***, and ***e*** signals are associated with the alternating PEG-PLA copolymer structures. Detailed peak assignments are provided in Table S2.

The chemical structures of PEG-PLA and PLA were further elucidated using FT-IR analysis (Fig. 1d). The resulting spectra displayed all the characteristic absorption bands associated with the PLA and PEG components, such as the $\nu_{C\text{-}H}$ of the PEG block at 2876–2882 cm^{-1} and the $\nu_{C=O}$ of the PLA block at 1729 cm^{-1}. Essentially, the amide bond of the polymers was confirmed by distinct peaks at 3500 cm^{-1} and 1529 cm^{-1}, which correspond to the $\nu_{N\text{-}H}$ and $\delta_{N\text{-}H}$ of the -NH group, respectively. Moreover, the signals at 3350–3450 cm^{-1} almost disappeared, implying a positive reaction between the terminal -OH and -NCO of the HDI coupling agent. These results support the successful synthesis of PEG-PLA and PLA, consistent with the ^{1}H NMR results. For more details on FT-IR absorption, please refer to our previous study [31]. The M_n, M_w, and Đ of all resulting samples were determined by GPC, with M_n ranging from 56,300–91,400 g mol^{-1} and Đ of approximately 1.6, thus confirming the successful synthesis of high M_n PEG-PLA and PLA bioplastics. The controlled composition was efficiently tailored by altering the feed ratio, and as shown in Fig. 1e, the retention time of each copolymer and homopolymer was recorded by GPC as only a single narrow retention peak in the uniform GPC retention time profiles. Thus, combined with the ^{1}H NMR and FT-IR spectra, PEG-PLA copolymers with sequence-controlled alternating and random structures and different compositions were confirmed, and a series of designed copolymers and homopolymers were fabricated as expected.

The macroscopic appearance of the specimens is shown in Fig. 1f. Random PEG-PLA copolymers and PLA homopolymers showed better transparency. UV-Vis spectroscopy demonstrated the transmittance values (Fig. S3), consistent with the macroscopic appearances of the samples.

3.2. Water durability of PEG-PLA multiblock copolymer films

Water and microorganisms predominantly attack hydrophilic molecular chains [38]. Therefore, increasing hydrophilicity can accelerate polymer biodegradation in marine environments by enhancing water absorption. PEG is crucial in the molecular design of PLA-based copolymers to transition from hydrophobic to hydrophilic, increasing potential "breaking points" [22]. To ensure PEG-PLA copolymers remain stable and durable in DI water, their behavior affected by hydrophilic components should be prioritized. This study explored the effects of alternating and random structures of PEG-PLA copolymers on their performance. As shown in Fig. S4, we compared the WUR of copolymers with different PLA chain segments. PLA segments shorter than 1000 g mol^{-1} gradually disintegrated in water after more than 4 h, while segments longer than 4000 g mol^{-1} exhibited WUR of less than 30%, potentially limiting their biodegradation. Copolymers with PLA chain lengths of 1500 and 2000 g mol^{-1} showed comparable WUR of approximately 180%. Considering the mechanical strength provided by longer PLA chains, PEG-PLA copolymers with PLA segments of 2000 and 3000 g mol^{-1} were chosen for a comparative study to identify the impact of sequence control.

Fig. 2b shows that copolymers with random structures and shorter PLA chain lengths show more rapid and higher water absorption, suggesting that the irregular arrangement of random chains and lower content of hydrophobic PLA facilitates water molecule diffusion. The corresponding data is summarized in Table S3. In contrast to PLA-*h*, PEG-PLA increased the water sensitivity, absorption rate, and capacity (Fig. 2c). The water contact angle (WCA) measurements (Fig. 2d) aligned with these results. The addition of PEG increased the density of polar ether bonds in the molecular chain compared with neat PLA-*h*. The oxygen atoms are highly electrophilic and can interact with water molecules through hydrogen bonding, thus improving the hydrophilicity of the PEG-PLA copolymer, resulting in a significant decrease in the WCA from 80.9° ± 2.3° (PLA_{3k}-*h*) to 38.3° ± 7.2° ($PEG_{4k}PLA_{2k}$-*r*). Further, we studied the materials after soaking in DI water at 22

Table 1
Characteristic data of conventional DSC analysis.

Samples	T_g[a] (°C)	T_c (°C)	ΔH_c (J g^{-1})	T_m (°C)	ΔH_m (J g^{-1})	X_c (%)
$PEG_{4k}PLA_{2k}$-*a*	– 42.5	22.1	9.23	61.1	10.94	10.76[c]
$PEG_{4k}PLA_{3k}$-*a*	– 36.3	42.9	16.40	82.3	15.92	40.18[d]
				122.2	4.87	
$PEG_{4k}PLA_{2k}$-*r*	– 30.6	25.1[b]	3.82[b]	57.5	3.85	3.83[c]
$PEG_{4k}PLA_{3k}$-*r*	– 18.5	31.8[b]	6.16[b]	65.6	6.53	13.07[d]
PLA_{2k}-*h*	45.6	-[e]	-[e]	-[e]	-[e]	-[e]
PLA_{3k}-*h*	50.4	-[e]	-[e]	-[e]	-[e]	-[e]

[a] Obtained from the second heating scan.
[b] Cold crystallization temperature and enthalpy obtained from the heating scan.
[c] The X_c was calculated by $\Delta H^0_{m,\ PEG}$ of 196.8 J g^{-1} [45].
[d] The X_c was calculated by $\Delta H^0_{m,\ PLA}$ of 93 J g^{-1} [46].
[e] No thermal transition was detected in the cooling or heating process.

± 0.5 °C for 6 months. The macroscopic appearance and microscopic morphology, as shown in Fig. 2e, indicate that all films remained almost complete. The chemical structure and molecular weight changes of the materials were further characterized using ^{1}H NMR, FT-IR, and GPC, with corresponding results added in the Supporting Information (Fig. S5, Table S4), and except for $PEG_{4k}PLA_{2k}$-*r*, the M_n of PLA-*h* decreased very small, while the remaining PEG-PLA copolymers maintained the M_n above 15,000 g mol^{-1}. The characteristic $\delta_{N\text{-}H}$ in FT-IR revealed that amide bonds were still present. Other results also confirmed that the stability of the materials in DI water is considerable.

3.3. Thermal properties and crystallinity of PEG-PLA multiblock copolymer films

The thermal and crystallization properties of the PEG-PLA copolymers and PLA homopolymers were investigated by DSC and XRD, respectively. The corresponding data are presented in Table 1. The integration of PEG into PLA decreased the rigidity of the copolymer because of the flexible ether bond and lower steric hindrance of PEG compared with the ester bonds and -CH_3 group of PLA, enhancing the mobility and arrangement of the molecular chains for increased crystallinity. Copolymers with alternating structures exhibited stronger crystallization, which is attributed to their high regularity and homogeneity. As displayed in Fig. 3**a,b**, PEG-PLA with an alternating structure showed a clear crystallization–melting transition compared with the amorphous thermal behavior of PLA-*h*, which showed no corresponding crystallization–melting transition, different from the amorphous thermal behavior of PLA-h. Introducing PEG units disrupts the PLA arrangements, with longer PLA units promoting better copolymer crystallization [39]. This effect increased the crystallization temperature (T_c), melting temperature (T_m), and enthalpy (ΔH) of the copolymers, especially with PLA3000. In addition, polymers with random structures showed lower T_c, T_m, and ΔH than those with alternating structures, with crystallization occurring during heating due to insufficient chain flexibility for crystalline stacking during the cooling process. This suggests that the random copolymer segments have poorer mobility and crystallization rates. As shown in Fig. 3**c**, the T_g of copolymers gradually decreased from 50.4 °C to − 42.5 °C with increasing PEG, allowing flexibility and low-temperature resistance. The crystallinity of biodegradable polyesters with relatively low T_g enables their development as thermoplastics. Blends of immiscible polymers showed two T_g values, while miscible polymers exhibited a single, composition-dependent T_g, indicating compatibility in amorphous regions [40]. These features suggest that short PLA chains could reduce PEG crystallinity while maintaining compatibility in the amorphous areas.

The XRD patterns in Fig. 3d show the diffraction peaks of the crystal structure of the samples with different compositions, further verifying the effect of PEG on the crystal structure of the copolymers. For PLA_{2k}-*h* and PLA_{3k}-*h*, broad diffraction peaks are present at 10–25° because of the scattering of molecular chains. In contrast, the PEG-PLA copolymers show sharp diffraction peaks typical of PLA at 16.60°, corresponding to the (110) or (200) planes of the orthorhombic crystals of the α-crystalline phase of PLA [41]. The intensity of the peaks indicates the introduced PEG induced an α-crystalline structure and improved the crystallinity of PLA. In contrast to $PEG_{4k}PLA_{3k}$, characteristic diffraction peaks of the PEG phases appear at 19.10° and 23.25° in $PEG_{4k}PLA_{2k}$ owing to the increase in the relative content of PEG; these peaks are attributed to the lattice planes of (115) and (016), respectively [42,43]. In conclusion, the diffraction peak locations did not change with the introduction of PEG, and the copolymers exhibited features of semi-crystalline polymers with similar crystal structures. The intensity of the corresponding peaks decreased, demonstrating that the alternating structure had stronger crystallizability than the random structure. Moreover, 2D WAXS analysis was utilized to illustrate the difference between the alternating and random structures of the copolymers (Fig. 3**e**), and the results were consistent with the XRD results. Considering the above DSC analysis, copolymers with random structures presented crystallization peaks during the second heating scan because a weaker crystallization capacity is required for a slower cooling rate. This supported the conclusions drawn from the XRD patterns.

To fully understand the crystallinity growth and spherulite size of PEG-PLA and PLA, POM was employed to monitor in situ crystal growth during the isothermal process. Optical micrographs were obtained after melting specimens and rapidly cooling them. Fig. 3**f(a'-c')** shows the isothermal crystallization of $PEG_{4k}PLA_{3k}$-*a* at 100 °C, where only PLA spherulites can grow. Initially, PLA nucleation occurred, forming tiny spherical crystals (Fig. 3**f(a',b')**). Over time, these crystals grew, but most remained imperfect at the end of crystallization (Fig. 3**f(c')**). In $PEG_{4k}PLA_{2k}$-*a* (Fig. 3**f(d')**), no crystals formed due to shorter PLA chains and higher PEG content. $PEG_{4k}PLA_{3k}$-*r* and $PEG_{4k}PLA_{2k}$-*r* showed similar results due to random chain segment arrangements (Fig. S6a-**c**). At 55 °C, $PEG_{4k}PLA_{3k}$-*a* showed smaller and densely arranged spherulite nuclei (Fig. 3**f(e',f')**). This rigidity promoted PEG nucleation but restricted the rate. Initial crystallization was attributable to PEG, with separate crystallization of PEG and PLA chains observed (Fig. 3**f(f')**). This indicates that the crystallization of the PEG and PLA chains occurred separately, which is consistent with the findings on diblock copolymers reported by Arnal et al. [44]. $PEG_{4k}PLA_{3k}$-*a* displayed the most rapid spherulitic growth, superior to that of $PEG_{4k}PLA_{2k}$-*a* (Fig. 3**f (g',h')**), $PEG_{4k}PLA_{3k}$-*r* (Fig. S6d-**f**), and $PEG_{4k}PLA_{2k}$-*r* (Fig. S6g-**i**), consistent with DSC results.

As a result, $PEG_{4k}PLA_{2k}$-*a* and $PEG_{4k}PLA_{3k}$-*a* displayed noticeable crystallization behaviors. The compatibility in the amorphous region and mutual restriction during crystallization were verified; alternating structures led to a lower WUR and superior mechanical properties, which were attributed to their strong crystallization ability and uniform molecular structure. Moreover, their crystallization behavior was strongly affected by the chain segment length, chain sequence distribution, and copolymer composition during the adjusted transition from amorphous to semi-crystalline structures, ultimately affecting their WUR ability and mechanical properties. The microstructure can be precisely controlled by tailoring the feed ratio and synthesis procedures, striking a balance between mechanical properties and biodegradability for DI water durability and tunable rapid biodegradability in seawater.

3.4. Thermal stability and dynamic viscoelastic properties of PEG-PLA multiblock copolymer films

The thermal stability of the PEG-PLA copolymers under a nitrogen atmosphere was evaluated using TGA, as shown in Fig. 4a. The DTGA curves are presented in Fig. S7. The corresponding data, such as the temperature of 5 % weight loss ($T_{d,\ 5\ \%}$) and maximum decomposition temperature ($T_{d,\ max}$), are listed in Table S5. The thermal decomposition profiles of the PEG-PLA copolymers and PLA homopolymers displayed

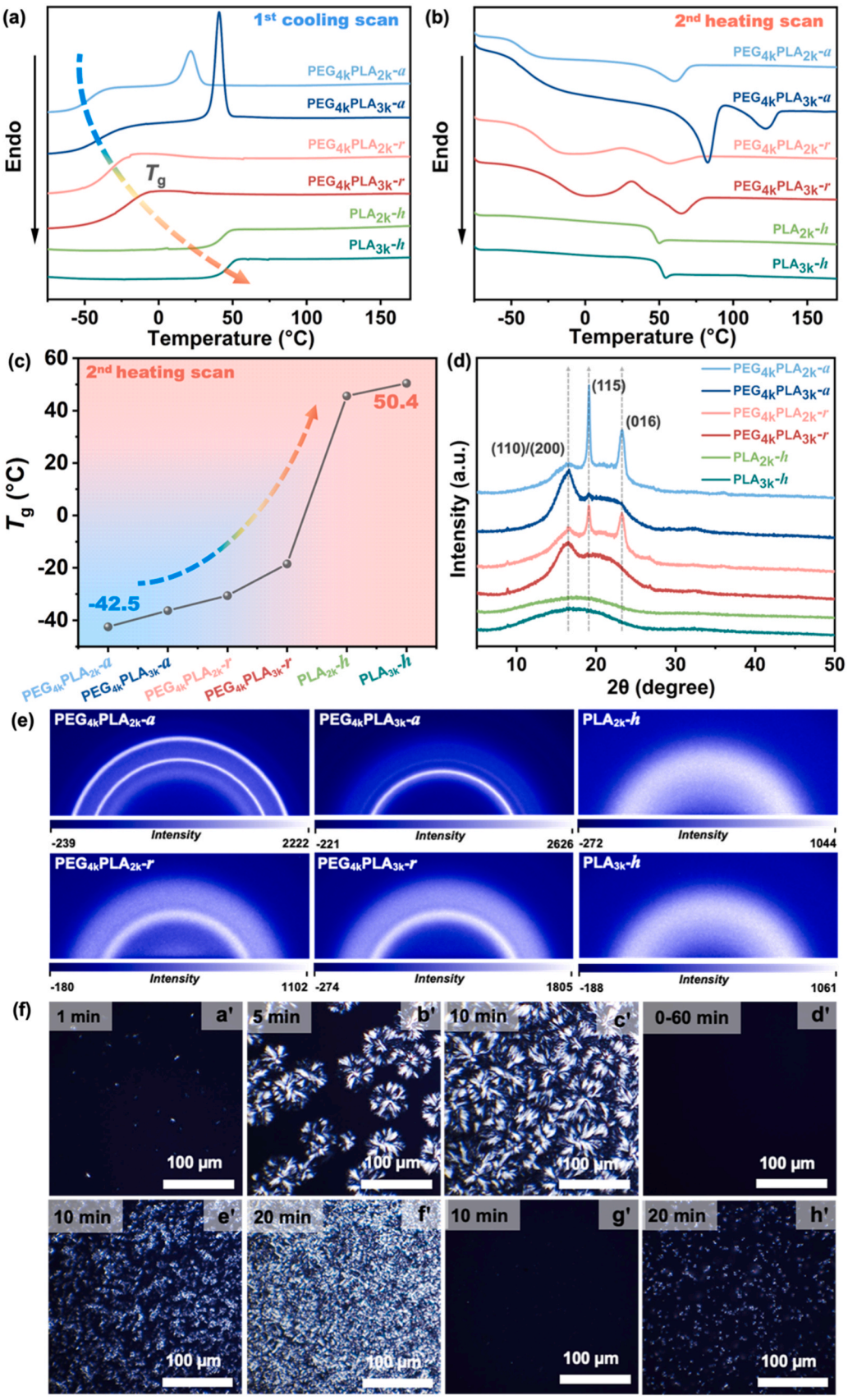

Fig. 3. DSC curves of PEG-PCL and PLA during the (a) first cooling and (b) second heating scan. (c) Transition of T_g with various structures and PLA contents. (d) 1D XRD and (e) 2D WAXS patterns of PEG-PLA and PLA. (f) POM images of $PEG_{4k}PLA_{3k}$-*a* (a'-c') and $PEG_{4k}PLA_{2k}$-*a* (d') crystallized isothermally at 100 °C; POM images of $PEG_{4k}PLA_{3k}$-*a* (e', f') and $PEG_{4k}PLA_{2k}$-*a* (g', h') crystallized isothermally at 55 °C.

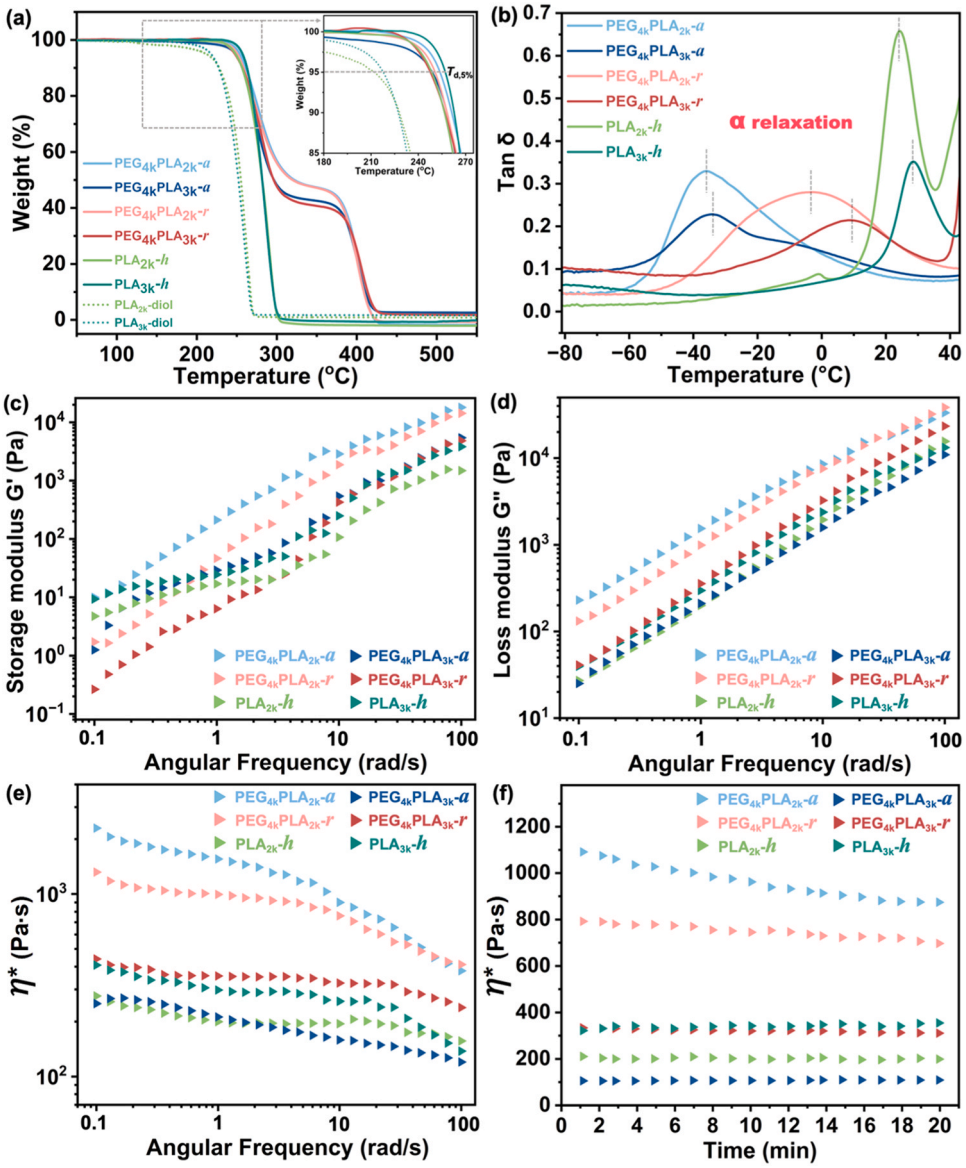

Fig. 4. (a) TGA curves of PEG-PLA and PLA. (b) Tan δ as a function of temperature for PEG-PLA and PLA recorded by DMA. (c) Dynamic storage modulus, (d) dynamic loss modulus, (e) complex viscosity, and (f) time-oscillation scanning curves of PEG-PLA and PLA at $T_r = 130$ °C.

$T_{d,\ max}$ values comparable to those of the prepolymers. With PEG incorporation, the curves showed a dual-stage thermal degradation corresponding to the distinct components. A slight decrease in $T_{d\ and\ max\text{-}PLA}$ compared with that of PLA-*h* was observed with longer PLA chain segments. In contrast, the PEG component remained stable and unaffected by the presence of PLA. The $T_{d\ max}$ values of the random copolymers were slightly higher than those of the alternating copolymers, possibly owing to longer chain segments in the random copolymers. All the copolymers demonstrated thermal stability up to 240 °C, with $T_{d,\ max}$ surpassing 400 °C, providing enhanced thermal stability for a wider processing window.

The variation in tan δ with temperature for the PEG-PLA and PLA was evaluated using DMA. In Fig. 4**b**, only a single relaxation peak on each of the tan δ curves was observed in the temperature range of − 80 °C to 40 °C, which was related to the T_g in the amorphous region of polymers. The introduction of PEG improved the mobility of PLA, and the α relaxation peak shifted to lower temperatures. In contrast to the alternating structures, the random structures presented higher T_g, corresponding to the DSC analysis results.

Dynamic viscoelastic parameters are essential for polymer processing techniques like melt spinning, injection, and extrusion molding [47]. The complex viscosity (η*), dynamic storage modulus (G'), and dynamic loss modulus (G") curves were measured using a rotational rheometer at 130 °C. As shown in Fig. 4**c-e**, all samples exhibited pseudoplasticity shear thinning behavior. The rheological properties varied with composition, with the low-frequency region reacting to large-scale rearrangements of the chain conformations and the high-frequency region reacting to limited chain segments [48]. The incorporated PEG may moderate shear thinning at high shear rates by reinforcing intermolecular interactions within the copolymer matrix. The minimal decrease in complex viscosity over time demonstrated good PEG-PLA and PLA thermal stability during early shear stages, which is crucial for processing applications (Fig. 4**f**).

3.5. *Mechanical properties of PEG-PLA multiblock copolymer films*

The mechanical performance of PEG-PLA copolymers is crucial for their practical application. Therefore, it is essential to understand their mechanical behavior under both dry and wet conditions based on the need for DI water durability. Similarly, we compared PEG-PLA with

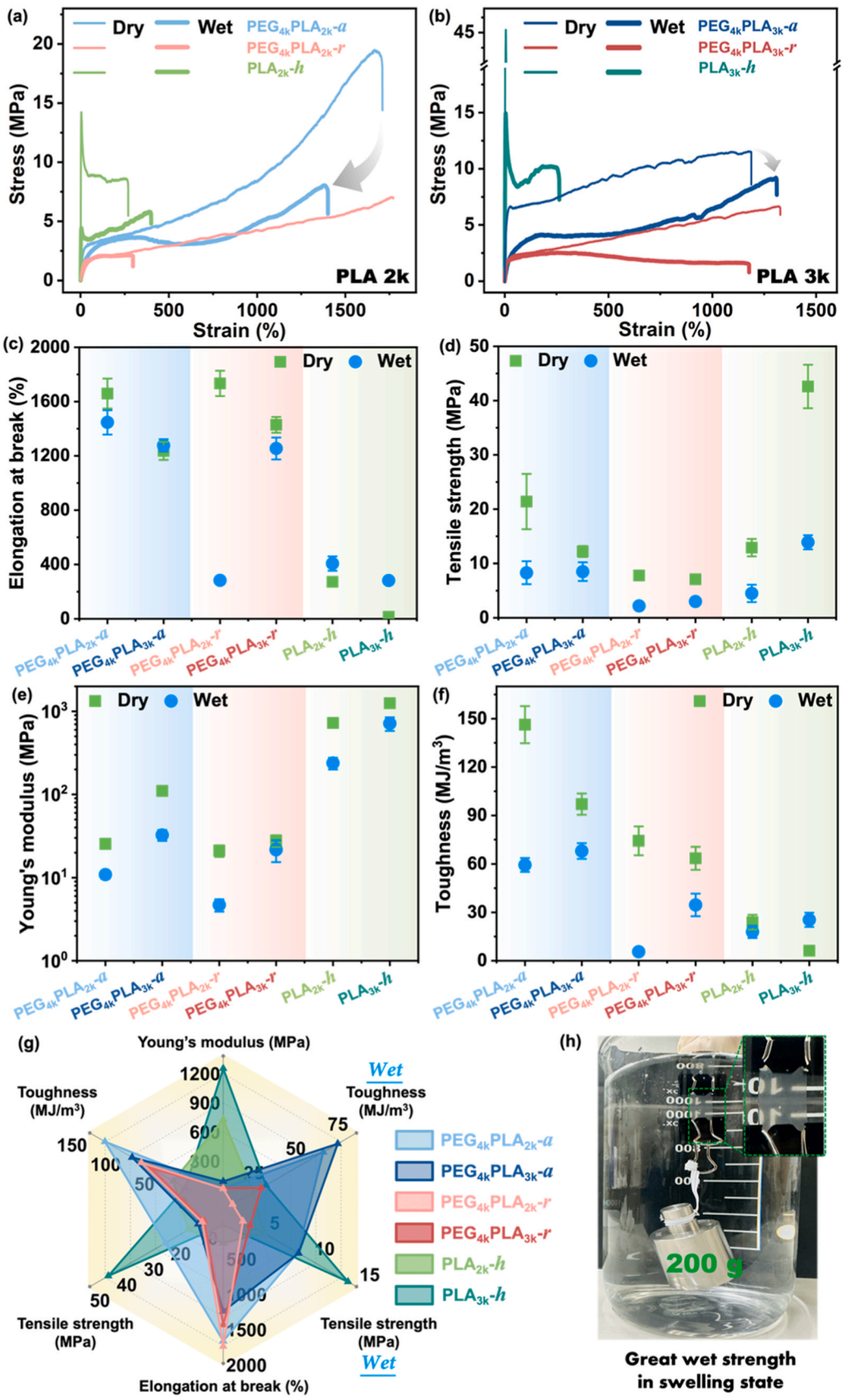

Fig. 5. Typical engineering stress–strain curves of PEG-PLA copolymers and PLA homopolymers with PLA 2k (a) and PLA 3k (b) chain segments in dry and wet states. (c) ε_b, (d) σ_m, (e) E', and (f) toughness of PEG-PLA and PLA in dry and wet states. (g) Comparative totalization of the mechanical properties of whole systems. (h) $PEG_{4k}PLA_{3k}$-*a* immersed in DI water at ambient atmosphere for 2 months and utilized for wet strength tests, as indicated by the green dotted line.

Table 2
Mechanical properties of PEG-PLA copolymers under different conditions.

Samples	Films state	Young's Modulus E (MPa)	Toughness (MJ/m^3)	Tensile Strength σ_m (MPa)	Elongation at break ε_b (%)
$PEG_{4k}PLA_{2k}$-*a*	Dry	21.5 ± 1.8	125.3 ± 11.5	21.4 ± 5.1	1659.3 ± 110.4
$PEG_{4k}PLA_{3k}$-*a*	Dry	91.9 ± 5.7	85.0 ± 6.6	9.2 ± 1.0	1236.7 ± 66.5
$PEG_{4k}PLA_{2k}$-*r*	Dry	17.2 ± 2.3	71.3 ± 8.3	7.8 ± 0.8	1734.0 ± 93.2
$PEG_{4k}PLA_{3k}$-*r*	Dry	23.2 ± 4.5	57.7 ± 7.1	7.1 ± 0.5	1428.6 ± 58.2
PLA_{2k}-*h*	Dry	726.2 ± 47.6	23.9 ± 4.6	12.9 ± 1.6	272.7 ± 4.4
PLA_{3k}-*h*	Dry	1253.1 ± 102.0	6.2 ± 2.1	42.6 ± 4.0	15.1 ± 3.7
$PEG_{4k}PLA_{2k}$-*a*	Wet	9.2 ± 1.2	59.4 ± 4.3	8.3 ± 2.1	1446.8 ± 89.8
$PEG_{4k}PLA_{3k}$-*a*	Wet	16.5 ± 2.9	68.0 ± 4.8	8.4 ± 1.7	1277.3 ± 45.6
$PEG_{4k}PLA_{2k}$-*r*	Wet	6.0 ± 0.8	5.6 ± 1.6	2.2 ± 0.2	283.8 ± 21.9
$PEG_{4k}PLA_{3k}$-*r*	Wet	21.8 ± 6.3	22.6 ± 7.0	3.0 ± 0.5	1254.2 ± 80.5
PLA_{2k}-*h*	Wet	238.5 ± 38.6	17.9 ± 3.8	4.5 ± 1.6	406.8 ± 52.3
PLA_{3k}-*h*	Wet	715.0 ± 133.4	25.4 ± 4.4	13.9 ± 1.3	282.5 ± 23.5

alternating structures and varying PLA chain lengths to tailor the PEG content. Typical engineering stress–strain curves are shown in Fig. S8, revealing that the mechanical properties of the copolymers with PLA chain lengths of less than 2000 g mol^{-1} were fragile in the wet state, which is inadequate to support the application requirements. Hence, copolymers with PLA chain lengths of 2000 and 3000 g mol^{-1} were selected for further comparative studies with alternating and random structures for a trade-off between biodegradability and mechanical properties. As illustrated in Fig. 5a, b, and data listed in Table 2, all PEG-PLA copolymers exhibited substantially improved flexibility and toughness compared to PLA-*h*. Despite a reduction in Young's modulus (*E'*), the mechanical requirements of various applications were satisfied. Detailed mechanical characteristics describing the mechanical attributes of copolymers in both dry and wet conditions, including the elongation at break (ε_b), maximum stress (σ_m), *E'* and toughness, are presented in Fig. 5c-f, respectively. An increase in PLA chain length from 2000 to 3000 g mol^{-1} produced a transition in the copolymer state from rubber-like to plastic-like, with a corresponding rise in *E'*, possibly attributable to enhanced crystallization ability.

In the dry state, alternating copolymers tend to have a more regular structure, leading to better crystallinity. This results in well-defined crystalline regions for the lower T_g that enhance mechanical strength and toughness [49]. However, in the wet state, the alternating-structure copolymers retained considerable mechanical properties, presenting increased ε_b and toughness, while the strength did not decrease significantly. This reinforcement might be due to water diffusion, resulting in an amorphous state of the PEG and PLA segments, which exhibit excellent compatibility and mobility, particularly for shorter PLA chain segments. This uniform dispersion of the chains prevents stress concentration, thereby enhancing the stretchability of the copolymers. This is also attributed to the regularity of crystallization and the formation of hydrogen bonds between water and the PEG in the chain segment, thus strengthening the intermolecular chain forces and supporting the mechanical strength.

A comprehensive summary of the mechanical behavior in various states is depicted in Fig. 5**g**, demonstrating the alternating structure with superior properties, and the introduction of PEG into PLA allows the bioplastic to develop sufficient potential for applications even in moist environments. As shown in Fig. 5**h**, $PEG_{4k}PLA_{3k}$-*a* was immersed in DI water at room temperature (22 ± 0.5 °C) for 2 months and still displayed exceptional wet strength. The Supporting Information **(Video 1)** demonstrates the corresponding wet strength in water.

Supplementary material related to this article can be found online at doi:10.1016/j.jhazmat.2024.134819.

3.6. Hydrolytic and enzymatic degradation of PEG-PLA multiblock copolymer films

Since this research aims to enhance the biodegradability of copolymers in marine environments, we must address the challenge of low microbial concentrations in seawater. If the PEG-PLA copolymer can undergo enzymatic biodegradation at lower enzyme (or microorganisms) concentrations, the possibility of marine biodegradation will significantly increase. Therefore, before conducting marine biodegradation experiments, we performed enzymatic degradation experiments with proteinase K. In our previous study, PEG-PLA copolymers with specific compositions exhibited pH-dependent degradation [31], specifically under alkaline conditions (pH 9). Because of its serine protease activity and broad substrate specificity, proteinase K effectively catalyzes PLA hydrolysis, similar to peptide bond cleavage in alanine-like PLA monomers. This enzymatic degradation, which is influenced by pH and temperature, occurs primarily through the interaction of nucleophilic residues of serine with ester bonds [50,51]. Such interactions lead to rapid and random ester bond cleavage in PLA. Given the similarity of the ester and amide bonds in PEG-PLA and PLA to peptide bonds, they are likewise susceptible to degradation, particularly in weakly alkaline marine environments. Consequently, we conducted hydrolytic (as a blank control group) and enzymatic degradation experiments of PEG-PLA and PLA without proteinase K in Tris-HCl buffer (pH = 8.5) at 37 °C for 120 h. The degradation tests in Tris-HCl buffer without proteinase K showed noticeable weight loss (<5%), except for the $PEG_{4k}PLA_{2k}$ copolymer. Fig. S10b and Fig. S9 show the corresponding microscopic results and hydrolytic degradation mechanisms. As polyurethanes are recognized to possess the structural characteristics of polyesters and polyamides, their sensitivity to hydrolytic degradation is identical to that of polyesters and polyamides. The urethane bond is also hydrolyzed with the facile hydrolysis of the ester group, but it is less susceptible, resulting in organic fragments (carboxylic acids, amines, or alcohols) [52,53].

0.2 mg mL^{-1} of proteinase K is typically used for enzymatic degradation reactions [54]. We first observed the behavior of the samples under this enzymatic degradation condition; however, all the samples dissolved in the buffer solution within 24 h. Hence, we adjusted the proteinase K concentration to an optimal concentration of 0.0125 mg mL^{-1}, considering the hydrophilic nature of the samples. This optimization was crucial because higher concentrations led to complete dissolution within 24 h, which overwhelmed the comparative analysis. The effects of the appropriate enzyme concentration on the degradation behavior are listed in Table S6. As shown in Fig. 6a and Fig. S10a, except for PLA-*h*, only $PEG_{4k}PLA_{3k}$-*a* still retained a minor residual weight. As a semi-crystalline copolymer, the reduced crystallinity and crystal size caused by the random structure promotes penetration of water molecules into the molecular chain to contact the ester and amide bonds, facilitating proteinase K access. Moreover, the WAC of PEG-PLA gradually decreased with shorter PLA chains, causing stronger interaction forces between the molecular chains and water. Consequently, both $PEG_{4k}PLA_{2k}$ copolymers were degraded entirely within 72 h, resulting in a transparent solution. In contrast, PLA_{2k}-*h* showed a weight loss of approximately 30 % compared to PLA_{3k}-*h*, which was attributed to its amorphous nature, increased WCA, and hydrophilicity. Fig. S10b shows the corresponding microscopic changes of materials after enzymatic degradation, consistent with the residue weight results. Fig. 6b shows a possible enzymatic degradation mechanism. Overall, enzymatic degradation by proteinase K was significantly faster than the slower hydrolytic degradation in the Tris-HCl buffer solution. The PEG units

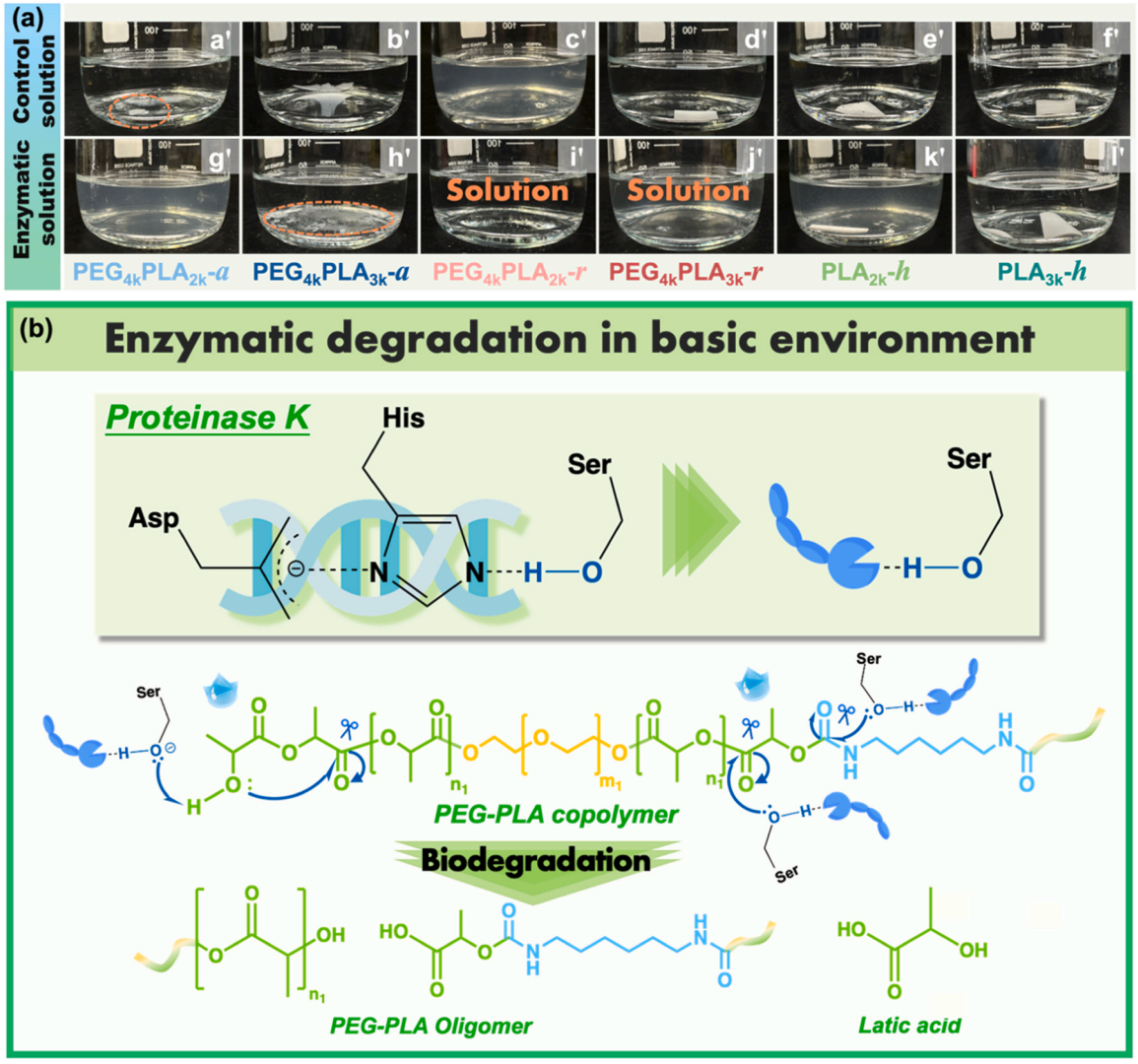

Fig. 6. (a) Enzymatic biodegradation of samples in proteinase K solution at 37 °C for 120 h. (b) Mechanism of proteinase K action on the PEG-PLA copolymer.

enhanced the hydrophilicity and promoted the biodegradability of the PEG-PLA copolymers.

3.7. Marine biodegradation of PEG-PLA multiblock copolymer films with seawater based on the BOD analysis

Inspired by the above results of the hydrolysis and rapid enzymatic degradation of PEG-PLA, we further assessed the biodegradability of the PEG-PLA copolymer and PLA homopolymers in seawater collected from Osaka Bay using the BOD analysis. In the standardized test set-up, aniline was used as a reference owing to its well-characterized biodegradation profile. The validity of the experimental approach against the OECD 306 [55] and ISO 18830:2016 [56] would be confirmed when the biodegradation tests conducted under these conditions yielded a half-life (t_{50}) of aniline of approximately 2–12 d and a final degradation rate of approximately 80 %, which is direct evidence of the biodegradability level of the target materials [57,58]. As shown in the curve for aniline degradation shown in Fig. 7**a**, the validity of the test results was verified based on the above theoretical considerations.

The corresponding test results are also shown in Fig. 7a. After 3 d, in addition to neat PLA-*h*, the consumption of O_2 started to increase gradually. Further, the biodegradation rate increased significantly after approximately 13 d. After 28 d, the biodegradation rates of $PEG_{4k}PLA_{2k}$-*r*, $PEG_{4k}PLA_{3k}$-*r*, $PEG_{4k}PLA_{2k}$-*a*, and $PEG_{4k}PLA_{3k}$-*a* were 72.63 %, 65.47 %, 60.61 %, and 53.11 %, respectively, which revealed that PEG-PLA was readily biodegradable in marine environments [59]; these results also markedly exceeded that of neat PLA-*h*. PEG-PLA, with a disordered structure and shorter PLA chain segments, showed a faster degradation t_{50} and higher biodegradation performance, which could be attributed to its lower crystallinity and higher hydrophilicity. The $PEG_{4k}PLA_{2k}$ copolymer with higher hydrophilicity also showed higher sensitivity in the initial stage of the degradation test (Fig. 7b). The degradation behavior was related to the Tris-HCl buffer and enzyme solutions, as described above. In addition, we compared the losses before and after degradation for all samples (Fig. S11). These results were consistent with the biodegradation performance, such as the weight loss of $PEG_{4k}PLA_{2k}$-*a* was 71.5%. Fig. 7c,d show the corresponding macroscopic and microscopic changes before and after the degradation of the samples, respectively. These results are consistent with the weight loss results, indicating that the improvement in the seawater biodegradation of PLA by the introduction of PEG was significant. Regarding the changes in M_n, it is evident from Fig. 7e that the retention time of PEG-PLA drastically increased with low M_n after 28 d of degradation in seawater. The signal of the random structure changed from a single peak to a triple peak because of the less regularity of the chain segments caused by the random copolymerization. The corresponding data are listed in Table S7. For example, the M_n of $PEG_{4k}PLA_{3k}$-*a* was reduced from 53,765 to 8733 g mol^{-1}, while Đ

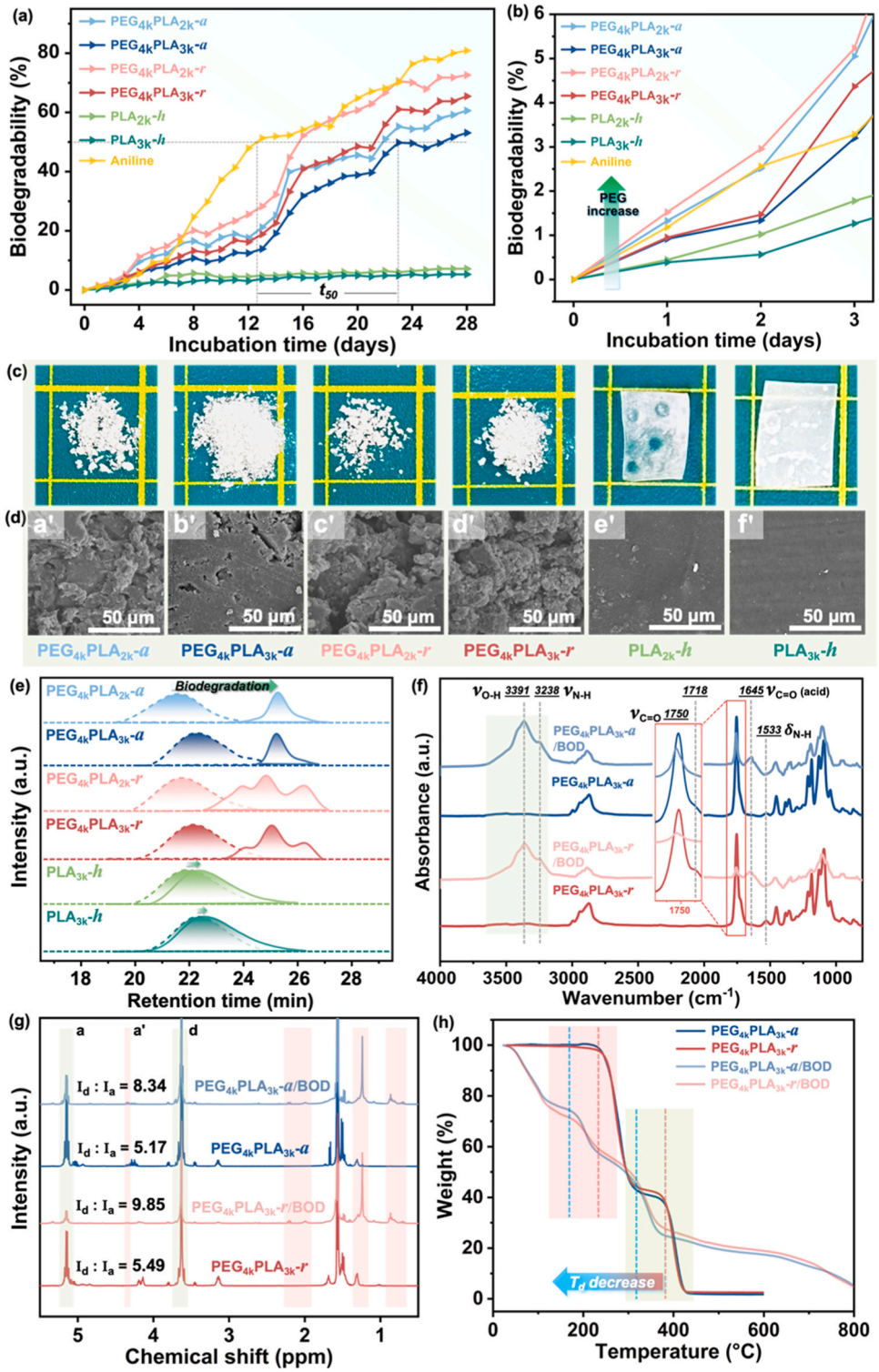

Fig. 7. (a) Comparison of the biodegradability of all samples after 28 d of seawater degradation. (b) Biodegradability of all samples in the initial stage of seawater degradation. After 28 d of seawater degradation, (c) macroscopic morphological changes of PEG-PLA and PLA films; (d) microscopic morphological changes of PEG-PLA and PLA films. recorded by SEM; (e) the retention time of all samples, the changes in the chemical structures and thermal stability of $PEG_{4k}PLA_{3k}$-*a* and $PEG_{4k}PLA_{3k}$-*r* demonstrated by (f) FT-IR, (g) ^{1}H NMR and (h) TGA, respectively.

decreased from 1.48 to 1.11. This further demonstrates that introducing PEG as a hydrophilic group into the backbone of PLA can improve its seawater biodegradability.

To understand the structure and composition, thermal properties, changes in thermal stability after degradation, and degradation mechanism of PEG-PLA, $PEG_{4k}PLA_{3k}$-*a,* and $PEG_{4k}PLA_{3k}$-*r* are considered as examples, FT-IR and ^{1}H NMR were carried out, and the detailed data are summarized in Table S7. In addition, there was a higher weight loss in the PLA component, causing severe degradation of the PLA chain segment from the side in seawater. Further, FT-IR was used to characterize changes in the functional groups of PEG-PLA (Fig. 7f). A distinct terminal hydroxyl peak appeared at 3391 cm^{-1} (both the end and

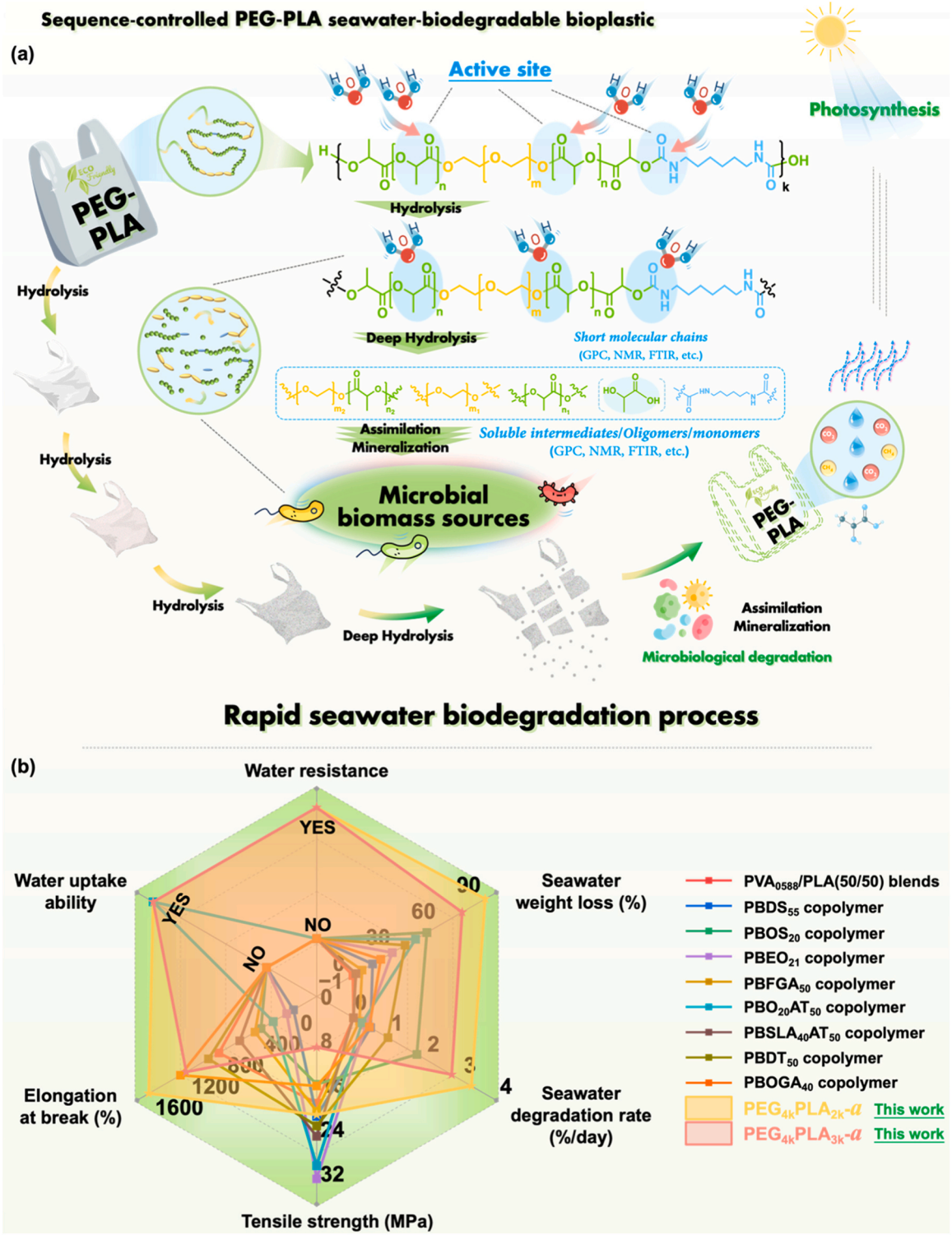

Fig. 8. (a) The proposal schematic illustration of the seawater biodegradation mechanism of PEG-PLA copolymers. (b) Comparison of the toughness, strain, water uptake ability, water durability, seawater weight loss, and seawater degradation rate with current research.

intramolecular ester exchange reaction of PLA resulted in increased -OH end groups, a detailed process referred to in Fig. S9) [52]. An overlapping peak corresponding to the stretching vibration of the amino group was observed at 3238 cm^{-1}. The carbonyl peak at 1750 cm^{-1} split into two stretching vibration peaks, and a new peak appeared at 1645 cm^{-1}, confirming the presence of free carboxyl groups after degradation. The disappearance of the bending vibration peak corresponding to the amide bond at 1533 cm^{-1} indicates that the ester and amide bonds that serve as the attack sites of water molecules were destroyed during the seawater degradation process, and the PEG-PLA bioplastic was rapidly degraded. In addition, as shown in Fig. 7g, the protons on the PEG methylene groups in the copolymer (***d***) were used as a reference to observe the change in the proton content of the PLA methine groups (***a***). The intensity ratio I_d/I_a of EG/LA changes from 5.17 to 8.34 and 5.49 to 9.85, respectively, implying that the PLA chain segments preferentially hydrolyzed in seawater. In contrast, the higher

increase in the random copolymer suggested that it was readily degraded, consistent with the results comparing the biodegradation properties and residual weight described above. This is consistent with the report by Feng et al. that during the degradation of poly (3-hydroxybutyrate-co-3-hydroxyvalerate), the amorphous region of the copolymer began to degrade first, followed by the crystalline region [60]. It can be seen in Fig. 7h that both alternating and random PEG-PLA had a sharp drop in their thermal stability after suffering from seawater degradation. The T_d of the PLA segment decreased by approximately 80 °C. Numata et al. identified that altering the ratios of the incorporated components in the copolymer chain affected their crystallinity and degradation rate [61]. Similarly, as shown in Fig. S12, for $PEG_{4k}PLA_{3k}$-*a*, the PLA crystallization peak appeared in the DSC cooling curve after degradation, and the ΔH_m corresponding to the melting peak increased from 4.87 to 19.75 J g^{-1}. While both the T_c and T_m of the PEG decreased, ΔH_c and ΔH_m increased, which suggests that after biodegradation, the molecular chains of the residue product were shorter. The mutual restriction between PEG and PLA weakened, allowing the latter to rearrange to increase the crystallinity. This implies that the degradation of seawater destroyed the chemical structure of PEG-PLA and modified its crystallization behavior. Table S8 presents comprehensive data on the thermal properties. Combining the stability of the chemical structure, microstructure, and molecular weight changes after soaking the material in DI water at 22 ± 0.5 °C for 6 months further demonstrates that incorporating PEG enhances the biodegradability of PLA in marine environments.

Fig. 8a presents a schematic of the hypothesized marine biodegradation mechanism for PEG-PLA copolymers [62,63]. The added PEG units in the PLA chain expand the interaction area between the ester and amide bonds and water molecules. This promotes the hydrogen bonding that accelerates the nucleophilic attack of water in marine environments with low temperatures, limited microorganisms, and high salinity. Consequently, this leads to an effectively tunable biodegradation rate of PEG-PLA containing varying EG/LA ratios. The superior overall performance of the PEG-PLA copolymers with elaborate alternating structures is demonstrated compared to reported marine-degradable polyesters [17,64–71] shown as radar plots (Fig. 8b); the specific data are summarized in Table S9. The alternating PEG-PLA structure provided a particularly outstanding marine biodegradation rate, has excellent stretchability both in wet and dry states, and shows simple, cost-effective manufacturing processes suitable for scaling up, making it a favorable alternative for marine-biodegradable polymers.

4. Conclusions

This study proposed the design of sequence-controlled PEG-PLA copolymer bioplastics with exceptional durability in DI water and rapid, tunable biodegradability in marine environments. The PEG-PLA copolymers were synthesized by ROP and coupling techniques with PLA and PEG as building blocks, achieving M_n exceeding 53,000 g mol^{-1}. The impact of the PEG content on the properties of PLA-based bioplastics was investigated. PEG-PLA exhibited tunable hydrophilicity (WAC from 80.9° ± 2.3° to 38.3° ± 7.2°) and water absorption (180.22% ± 0.21% to 5.11% ± 0.17%). $PEG_{4k}PLA_{2k}$-*a* presented excellent mechanical properties in both wet and dry states, with a maximum elongation at break and strength of 1446.8% ± 89.9% and 8.3 ± 2.1 MPa, respectively. The introduction of PEG increased the flexibility of the PLA molecular chain, reducing T_g from 50.4 °C to − 42.5 °C. With its well-organized chain structure, the alternating structure exhibited a lower T_g and stable rheological properties suitable for processing. In addition, PEG-PLA showed enhanced biodegradability with the incorporated PEG; $PEG_{4k}PLA_{2k}$ was biodegraded entirely in 120 h, even at a low proteinase K concentration of 0.0125 g mol^{-1}. The degradation mechanism prioritized the PLA segments within the PEG-PLA copolymer, as confirmed by comprehensive characterization techniques, including FT-IR, ^1H NMR, SEM, and GPC. The biodegradability by the OECD 306 reached 72.63%, as verified by quantitative 28-day BOD analysis. This proves that bioplastic has the potential for rapid chain scission in marine environments. Consequently, this study illustrated the trade-offs between PEG as a building unit in modifying PLA regarding thermal behavior, mechanical properties, DI water durability, and marine biodegradability. Elaborate PEG-PLA bioplastics can shed light on developing the next generation of tunable, fast marine-biodegradable, and renewable high-performance green materials for packaging, medical, and agricultural applications and address marine plastic pollution.

Environmental impliation

Emerging high-performance marine-biodegradable plastics are widely considered the ideal strategy to address marine plastic pollution. However, the complex and harsh conditions of the marine environment severely inhibit the biodegradability of plastics. To accelerate polymer degradation in the ocean, bioplastics have been designed by structurally incorporating hydrophilic PEG units into bio-based PLA, yielding PEG-PLA copolymers with either sequence-controlled alternating or random structures. These copolymers exhibit tunable and superior mechanical properties, and undergo rapid yet tunable biodegradation in seawater within 28 days, offering a potential solution for tackling marine plastic pollution.

CRediT authorship contribution statement

Yu-I Hsu: Writing – review & editing, Visualization, Methodology, Funding acquisition, Conceptualization. **Manjie He:** Writing – original draft, Methodology, Investigation, Conceptualization. **Hiroshi Uyama:** Writing – review & editing, Supervision, Funding acquisition.

Declaration of Competing Interest

The authors declare that they have no known competing financial interests or personal relationships that could have appeared to influence the work reported in this paper.

Data availability

Data will be made available on request.

Acknowledgments

This work was supported by Japan Science and Technology Agency Grants (JPMJPF2218), the Environment Research and Technology Development Fund JPMEERF21S11900 of the Environmental Restoration and Conservation Agency of Japan, JSPS KAKENHI Grants (22K21348), JSPS KAKENHI Grants (23H02024), JST PRESTO Grants (JPMJPR23N4), and JST SPRING Grants (JPMJSP2138). We thank the Analytical Instrument Facility at Graduate School of Science, Osaka university for the organic element analyses.

Appendix A. Supporting information

Supplementary data associated with this article can be found in the online version at doi:10.1016/j.jhazmat.2024.134819.

References

[1] Jambeck, J.R., Geyer, R., Wilcox, C., Siegler, T.R., Perryman, M., Andrady, A., et al., 2015. Plastic waste inputs from land into the ocean. Science 347, 768–771. https://doi.org/10.1126/science.1260352.
[2] Albertsson, A.-C., Hakkarainen, M., 2017. Designed to degrade. Science 358, 872–873. https://doi.org/10.1126/science.aap8115.
[3] Lim, X., 2021. Microplastics are everywhere — but are they harmful. Nature 593, 22–25. https://doi.org/10.1038/d41586-021-01143-3.
[4] Huang, W., Song, B., Liang, J., Niu, Q., Zeng, G., Shen, M., et al., 2021. Microplastics and associated contaminants in the aquatic environment: a review on

their ecotoxicological effects, trophic transfer, and potential impacts to human health. J Hazard Mater 405, 124187. https://doi.org/10.1016/j.jhazmat.2020.124187.
[5] Luo, D., Chu, X., Wu, Y., Wang, Z., Liao, Z., Ji, X., et al., 2024. Micro- and nano-plastics in the atmosphere: a review of occurrence, properties and human health risks. J Hazard Mater 465, 133412. https://doi.org/10.1016/j.jhazmat.2023.133412.
[6] Worm, B., Lotze, H.K., Jubinville, I., Wilcox, C., Jambeck, J., 2017. Plastic as a persistent marine pollutant. Annu Rev Environ Resour 42, 1–26. https://doi.org/10.1146/annurev-environ-102016-060700.
[7] Haward, M., 2018. Plastic pollution of the world's seas and oceans as a contemporary challenge in ocean governance. Nat Commun 9, 667. https://doi.org/10.1038/s41467-018-03104-3.
[8] Manfra, L., Marengo, V., Libralato, G., Costantini, M., De Falco, F., Cocca, M., 2021. Biodegradable polymers: a real opportunity to solve marine plastic pollution? J Hazard Mater 416, 125763. https://doi.org/10.1016/j.jhazmat.2021.125763.
[9] Karamanlioglu, M., Preziosi, R., Robson, G.D., 2017. Abiotic and biotic environmental degradation of the bioplastic polymer poly(lactic acid): A review. Polym Degrad Stab 137, 122–130. https://doi.org/10.1016/j.polymdegradstab.2017.01.009.
[10] Yu, J., Xu, S., Liu, B., Wang, H., Qiao, F., Ren, X., et al., 2023. PLA bioplastic production: from monomer to the polymer. Eur Polym J 193, 112076. https://doi.org/10.1016/j.eurpolymj.2023.112076.
[11] Wang, G.-X., Huang, D., Ji, J.-H., Völker, C., Wurm, F.R., 2021. Seawater-degradable polymers—fighting the marine plastic pollution. Adv Sci 8, 2001121. https://doi.org/10.1002/advs.202001121.
[12] Bagheri, A.R., Laforsch, C., Greiner, A., Agarwal, S., 2017. Fate of so-called biodegradable polymers in seawater and freshwater. Glob Chall 1, 1700048. https://doi.org/10.1002/gch2.201700048.
[13] Haider, T.P., Völker, C., Kramm, J., Landfester, K., Wurm, F.R., 2019. Plastics of the future? The impact of biodegradable polymers on the environment and on society. Angew Chem Int Ed 58, 50–62. https://doi.org/10.1002/anie.201805766.
[14] Sun, H., Liang, Y., Thompson, M.P., Gianneschi, N.C., 2021. Degradable polymers via olefin metathesis polymerization. Prog Polym Sci 120, 101427. https://doi.org/10.1016/j.progpolymsci.2021.101427.
[15] Stubbs, C.J., Worch, J.C., Prydderch, H., Wang, Z., Mathers, R.T., Dobrynin, A.V., et al., 2022. Sugar-based polymers with stereochemistry-dependent degradability and mechanical properties. J Am Chem Soc 144, 1243–1250. https://doi.org/10.1021/jacs.1c10278.
[16] Hu, C., Pang, X., Chen, X., 2022. Self-switchable polymerization: a smart approach to sequence-controlled degradable copolymers. Macromolecules 55, 1879–1893. https://doi.org/10.1021/acs.macromol.2c00085.
[17] Huang, D., Hu, Z.-D., Liu, T.-Y., Lu, B., Zhen, Z.-C., Wang, G.-X., et al., 2020. Seawater degradation of PLA accelerated by water-soluble PVA. E-Polym 20, 759–772. https://doi.org/10.1515/epoly-2020-0071.
[18] Chen, G., Xu, L., Zhang, P., Chen, B., Wang, G., Ji, J., et al., 2020. Seawater degradable triboelectric nanogenerators for blue energy. Adv Mater Technol 5, 2000455. https://doi.org/10.1002/admt.202000455.
[19] Kim, H.J., Hillmyer, M.A., Ellison, C.J., 2021. Enhanced polyester degradation through transesterification with salicylates. J Am Chem Soc 143, 15784–15790. https://doi.org/10.1021/jacs.1c07229.
[20] Xu, W., Ma, C., Ma, J., Gan, T., Zhang, G., 2014. Marine biofouling resistance of polyurethane with biodegradation and hydrolyzation. ACS Appl Mater Interfaces 6, 4017–4024. https://doi.org/10.1021/am4054578.
[21] Wang, S., Lydon, K.A., White, E.M., Grubbs, J.B.I., Lipp, E.K., Locklin, J., et al., 2018. Biodegradation of poly(3-hydroxybutyrate-co-3-hydroxyhexanoate) plastic under anaerobic sludge and aerobic seawater conditions: gas evolution and microbial diversity. Environ Sci Technol 52, 5700–5709. https://doi.org/10.1021/acs.est.7b06688.
[22] Rheinberger, T., Wolfs, J., Paneth, A., Wurm, F., et al., 2021. RNA-inspired and accelerated degradation of polylactide in seawater. J Am Chem Soc 143, 16673–16681.
[23] Meereboer, K.W., Misra, M., Mohanty, A.K., 2020. Review of recent advances in the biodegradability of polyhydroxyalkanoate (PHA) bioplastics and their composites. Green Chem 22, 5519–5558. https://doi.org/10.1039/D0GC01647K.
[24] Saravanan, K., Umesh, M., Kathirvel, P., 2022. Microbial polyhydroxyalkanoates (PHAs): a review on biosynthesis, properties, fermentation strategies and its prospective applications for sustainable future. J Polym Environ 30, 4903–4935. https://doi.org/10.1007/s10924-022-02562-7.
[25] D'souza, A.A., Shegokar, R., 2016. Polyethylene glycol (PEG): a versatile polymer for pharmaceutical applications. Expert Opin Drug Deliv 13, 1257–1275. https://doi.org/10.1080/17425247.2016.1182485.
[26] Wolf, T., Steinbach, T., Wurm, F., 2015. A library of well-defined and water-soluble poly(alkyl phosphonate)s with adjustable hydrolysis. Macromolecules 48, 3853–3863. https://doi.org/10.1021/acs.macromol.5b00897.
[27] Rosenboom, J.-G., Langer, R., Traverso, G., 2022. Bioplastics for a circular economy. Nat Rev Mater 7, 117–137. https://doi.org/10.1038/s41578-021-00407-8.
[28] Xiao, R.Z., Zeng, Z.W., Zhou, G.L., Wang, J.J., Li, F.Z., Wang, A.M., 2010. Recent advances in PEG–PLA block copolymer nanoparticles. Int J Nanomed 5 1057–1065. https://doi.org/10.2147/IJN.S14912.
[29] Ulbrich, K., Holá, K., Šubr, V., Bakandritsos, A., Tuček, J., Zbořil, R., 2016. Targeted drug delivery with polymers and magnetic nanoparticles: covalent and noncovalent approaches, release control, and clinical studies. Chem Rev 116, 5338–5431. https://doi.org/10.1021/acs.chemrev.5b00589.
[30] Ben-Shabat, S., Kumar, N., Domb, A.J., 2006. PEG-PLA block copolymer as potential drug carrier: preparation and characterization. Macromol Biosci 6, 1019–1025. https://doi.org/10.1002/mabi.200600165.
[31] He, M., Hsu, Y.-I., Uyama, H., 2024. Design of novel poly(L-lactide)-based shape memory multiblock copolymers for biodegradable esophageal stent application. Appl Mater Today 36, 102057. https://doi.org/10.1016/j.apmt.2024.102057.
[32] Liu, J., Mattiasson, B., 2002. Microbial BOD sensors for wastewater analysis. Water Res 36, 3786–3802. https://doi.org/10.1016/S0043-1354(02)00101-X.
[33] Williams, D.F., 1981. Enzymic hydrolysis of polylactic acid. Eng Med 10, 5–7. https://doi.org/10.1243/EMED_JOUR_1981_010_004_02.
[34] Reeve, M.S., McCarthy, S.P., Downey, M.J., Gross, R.A., 1994. Polylactide stereochemistry: effect on enzymic degradability. Macromolecules 27, 825–831. https://doi.org/10.1021/ma00081a030.
[35] Garland, E.M., Tozzolino, P., Dutrieux, E., 1998. Biodegradation of Chemicals in the Marine Environment: Towards Harmonised Protocols. SPE Int. Conf. Heal. Saf. Environ. Oil Gas Explor. Prod. https://doi.org/10.2118/46595-MS.
[36] Kasuya, K., Takagi, K., Ishiwatari, S., Yoshida, Y., Doi, Y., 1998. Biodegradabilities of various aliphatic polyesters in natural waters. Polym Degrad Stab 59, 327–332. https://doi.org/10.1016/S0141-3910(97)00155-9.
[37] He, M.-J., Xiao, W.-X., Xie, H., Fan, C.-J., Du, L., Deng, X.-Y., et al., 2017. Facile fabrication of ternary nanocomposites with selective dispersion of multi-walled carbon nanotubes to access multi-stimuli-responsive shape-memory effects. Mater Chem Front 1, 343–353. https://doi.org/10.1039/C6QM00047A.
[38] Du, Y., Liu, X., Dong, X., Yin, Z., 2022. A review on marine plastisphere: biodiversity, formation, and role in degradation. Comput Struct Biotechnol J 20, 975–988. https://doi.org/10.1016/j.csbj.2022.02.008.
[39] Saeidlou, S., Huneault, M.A., Li, H., Park, C.B., 2012. Poly(lactic acid) crystallization. Prog Polym Sci 37, 1657–1677. https://doi.org/10.1016/j.progpolymsci.2012.07.005.
[40] Imre, B., Pukánszky, B., 2013. Compatibilization in bio-based and biodegradable polymer blends. Eur Polym J 49, 1215–1233. https://doi.org/10.1016/j.eurpolymj.2013.01.019.
[41] Jia, L., Zhang, W.-C., Tong, B., Yang, R.-J., 2018. Crystallization, mechanical and flame-retardant properties of poly(lactic acid) composites with DOPO and DOPO-POSS. Chin J Polym Sci 36, 871–879. https://doi.org/10.1007/s10118-018-2098-7.
[42] Lee, J.S., Taghavimehr, M., Montazami, R., Green, M.D., 2022. Synthesis and characterization of Poly(ethylene glycol)-based segmented ionenes block copolymer with aliphatic or DABCO hard segments. Polymer 242, 124543. https://doi.org/10.1016/j.polymer.2022.124543.
[43] Hoogsteen, W., Postema, A.R., Pennings, A.J., Ten Brinke, G., Zugenmaier, P., 1990. Crystal structure, conformation and morphology of solution-spun poly(L-lactide) fibers. Macromolecules 23, 634–642. https://doi.org/10.1021/ma00204a041.
[44] Arnal, M.L., Boissé, S., Müller, A.J., Meyer, F., Raquez, J.-M., Dubois, P., 2016. R.E. Prud`homme, Interplay between poly(ethylene oxide) and poly(L-lactide) blocks during diblock copolymer crystallization. CrystEngComm 18, 3635–3649. https://doi.org/10.1039/C6CE00330C.
[45] Pielichowska, K., Nowak, M., Szatkowski, P., Macherzyńska, B., 2016. The influence of chain extender on properties of polyurethane-based phase change materials modified with graphene. Appl Energy 162, 1024–1033. https://doi.org/10.1016/j.apenergy.2015.10.174.
[46] Fischer, E.W., Sterzel, H.J., Wegner, G., 1973. Investigation of the structure of solution grown crystals of lactide copolymers by means of chemical reactions. Kolloid-Z U Z Polym 251, 980–990. https://doi.org/10.1007/BF01498927.
[47] Mondschein, R.J., Dennis, J.M., Liu, H., Ramakrishnan, R.K., Nazarenko, S., Turner, S.R., et al., 2017. Synthesis and characterization of amorphous bibenzoate (Co)polyesters: permeability and rheological performance. Macromolecules 50, 7603–7610. https://doi.org/10.1021/acs.macromol.7b01595.
[48] Ahmad, N.M., Lovell, P.A., Underwood, S.M., 2001. Viscoelastic properties of branched polyacrylate melts. Polym Int 50, 625–634. https://doi.org/10.1002/pi.672.
[49] Huang, C.-C., Du, M.-X., Zhang, B.-Q., Liu, C.-Y., 2022. Glass transition temperatures of copolymers: molecular origins of deviation from the linear relation. Macromolecules 55, 3189–3200. https://doi.org/10.1021/acs.macromol.1c02287.
[50] Kawai, F., Nakadai, K., Nishioka, E., Nakajima, H., Ohara, H., Masaki, K., et al., 2011. Different enantioselectivity of two types of poly(lactic acid) depolymerases toward poly(l-lactic acid) and poly(d-lactic acid). Polym Degrad Stab 96, 1342–1348. https://doi.org/10.1016/j.polymdegradstab.2011.03.022.
[51] Tsuji, H., Miyauchi, S., 2001. Enzymatic hydrolysis of poly(lactide)s: effects of molecular weight, l-lactide content, and enantiomeric and diastereoisomeric polymer blending. Biomacromolecules 2, 597–604. https://doi.org/10.1021/bm010048k.
[52] Macocinschi, D., Filip, D., Zaltariov, M.F., Varganici, C.D., 2015. Thermal and hydrolytic stability of silver nanoparticle polyurethane biocomposites for medical applications. Polym Degrad Stab 121, 238–246. https://doi.org/10.1016/j.polymdegradstab.2015.09.017.
[53] Magnin, A., Pollet, E., Phalip, V., Avérous, L., 2020. Evaluation of biological degradation of polyurethanes. Biotechnol Adv 39, 107457. https://doi.org/10.1016/j.biotechadv.2019.107457.
[54] Yamashita, K., Kikkawa, Y., Kurokawa, K., Doi, Y., 2005. Enzymatic degradation of poly(l-lactide) film by proteinase K: quartz crystal microbalance and atomic force microscopy study. Biomacromolecules 6, 850–857. https://doi.org/10.1021/bm049395v.

[55] Ott, A., Martin, T.J., Whale, G.F., Snape, J.R., Rowles, B., Galay-Burgos, M., et al., 2019. Improving the biodegradability in seawater test (OECD 306). Sci Total Environ 666, 399–404. https://doi.org/10.1016/j.scitotenv.2019.02.167.
[56] The British Standards Institution (BSI). 2016 BS ISO 18830:2016 Plastics. Determination of aerobic biodegradation of non-floating plastic materials in a seawater/sandy sediment interface. Method by measuring the oxygen demand in closed respirometer, pp. 1–18. London, UK: BSI.
[57] Strotmann, U., Reuschenbach, P., Schwarz, H., Pagga, U., 2004. Development and evaluation of an online CO_2 evolution test and a multicomponent biodegradation test system. Appl Environ Microbiol 70, 4621–4628. https://doi.org/10.1128/AEM.70.8.4621-4628.2004.
[58] Nakayama, A., Yamano, N., Kawasaki, N., 2019. Biodegradation in seawater of aliphatic polyesters. Polym Degrad Stab 166, 290–299. https://doi.org/10.1016/j.polymdegradstab.2019.06.006.
[59] López-Ibáñez, S., Beiras, R., 2022. Is a compostable plastic biodegradable in the sea? A rapid standard protocol to test mineralization in marine conditions. Sci Total Environ 831, 154860. https://doi.org/10.1016/j.scitotenv.2022.154860.
[60] Feng, L., Wang, Y., Inagawa, Y., Kasuya, K., Saito, T., Doi, Y., et al., 2004. Enzymatic degradation behavior of comonomer compositionally fractionated bacterial poly(3-hydroxybutyrate-*co*-3-hydroxyvalerate)s by poly(3-hydroxyalkanoate) depolymerases isolated from *Ralstonia pickettii* T1 and *Acidovorax* sp. TP4. Polym Degrad Stab 84, 95–104. https://doi.org/10.1016/j.polymdegradstab.2003.09.016.
[61] Numata, K., Kikkawa, Y., Tsuge, T., Iwata, T., Doi, Y., Abe, H., 2005. Enzymatic degradation processes of poly[(R)-3-hydroxybutyric acid] and poly[(R)-3-hydroxybutyric acid-co-(R)-3-hydroxyvaleric acid] single crystals revealed by atomic force microscopy: effects of molecular weight and second-monomer composition on erosion rates. Biomacromolecules 6, 2008–2016. https://doi.org/10.1021/bm0501151.
[62] Hakkarainen, M., 2002. Aliphatic Polyesters: Abiotic and Biotic Degradation and Degradation Products. In: Degradable Aliphatic Polyesters. Springer, Berlin, Heidelberg, pp. 113–138. https://doi.org/10.1007/3-540-45734-8_4.
[63] Inkinen, S., Hakkarainen, M., Albertsson, A.-C., Södergård, A., 2011. From lactic acid to poly(lactic acid) (PLA): characterization and analysis of PLA and its precursors. Biomacromolecules 12, 523–532. https://doi.org/10.1021/bm101302t.
[64] Zhu, T., Wang, L., Lu, Y., Wei, Z., et al., 2024. Rapid marine degradable poly (butylene oxalate) by introducing promotion building blocks, 132791-132807 J Hazard Mater 462. https://doi.org/10.1016/j.jhazmat.2023.132791.
[65] Liu, T., Huang, D., Xu, P., Lu, B., Zhen, Z., Wang, G., et al., 2022. Study on composting and seawater degradation properties of diethylene glycol-modified poly(butylene succinate) copolyesters. e-Polym 22, 615–626. https://doi.org/10.1515/epoly-2022-0057.
[66] Luan, Q., Hu, H., Jiang, X., Lin, C., Zhang, X., Wang, Q., et al., 2023. Melt polycondensation of poly (butylene oxalate-co-succinate) with great potential in curbing marine plastic pollution. J Hazard Mater 457, 131801. https://doi.org/10.1016/j.jhazmat.2023.131801.
[67] Ding, Y., Huang, D., Ai, T., Zhang, C., Chen, Y., Luo, C., et al., 2021. Bio-based poly (butylene furandicarboxylate-co-glycolate) copolyesters: synthesis, properties, and hydrolysis in different aquatic environments for water degradation application. ACS Sustain Chem Eng 9, 1254–1263. https://doi.org/10.1021/acssuschemeng.0c07351.
[68] Luan, Q., Hu, H., Ouyang, X., Jiang, X., Lin, C., Zhu, H., et al., 2024. New modifications of PBAT by a small amount of oxalic acid: Fast crystallization and enhanced degradation in all natural environments. J Hazard Mater 465, 133475. https://doi.org/10.1016/j.jhazmat.2024.133475.
[69] Liu, T.-Y., Huang, D., Xu, P.-Y., Lu, B., Wang, G.-X., Zhen, Z.-C., et al., 2022. Biobased seawater-degradable poly(butylene succinate-l-lactide) copolyesters: exploration of degradation performance and degradation mechanism in natural seawater. ACS Sustain Chem Eng 10, 3191–3202. https://doi.org/10.1021/acssuschemeng.1c07176.
[70] Tian, Y., Hu, H., Chen, C., Li, F., Bin Ying, W., Zheng, L., et al., 2022. Enhanced seawater degradation through copolymerization with diglycolic acid: synthesis, microstructure, degradation mechanism and modification for antibacterial packaging. Chem Eng J 447, 137535. https://doi.org/10.1016/j.cej.2022.137535.
[71] Hu, H., Li, J., Tian, Y., Chen, C., Li, F., Ying, W.B., et al., 2021. Experimental and theoretical study on glycolic acid provided fast bio/seawater-degradable poly (butylene succinate-co-glycolate). ACS Sustain Chem Eng 9, 3850–3859. https://doi.org/10.1021/acssuschemeng.0c08939.